

Binary Black Holes population synthesis based on the current LVK observations

Mehdi El Bouhaddouti ^{1,*}, Ilias Cholis ^{1,†} and Muhsin Aljaf ^{1,‡}

¹*Department of Physics, Oakland University, Rochester, Michigan, 48309, U.S.A*

The ongoing observations from ground based gravitational-wave observatories have led to the detection of more than a hundred merger events between black holes. We use the LIGO-Virgo-KAGRA (LVK) observations from 2015 to early 2024, to test the population synthesis of these merging binaries; which will allow us to probe the formation mechanisms and environments of these black holes. We test if the current sample of binary black holes can be explained only by the merger of black holes coming from the collapse of the cores of massive stars, i.e. as just first generation black holes merging with each other. Those black holes' masses will roughly follow a power-law distribution. We also test if in addition to the merger between first generation black holes, there is evidence for a second population of black hole binaries in which at least one the binaries' members is the product of an earlier merger between black holes. These binaries are typically referred to as signals of hierarchical mergers. Such a population can possibly explain the observation of very massive black hole binaries by the LVK collaboration. We find that the LVK observations give a statistical preference in log-likelihood of up to $-2\Delta\ln\mathcal{L} = -150$ or in log-Bayes factor of up to $\ln\text{BF} = 71$, for the full sample of black hole binaries originating from a combination of black holes following a power-law distribution and black holes from hierarchical mergers. The ratio of black holes following a power-law mass-distribution to a mass-distribution expected from hierarchical mergers is found to be as high as one-to-one. We also consider that some of the LVK black hole merging binaries are the result of primordial black holes (PBHs), merging inside dark matter halos and in the intergalactic medium. Adding a third population is preferred. Compared to a simple first generation population we get $-2\Delta\ln\mathcal{L} = -216$ and $\ln\text{BF} = 97$. We find that a few % of the observed LVK events can be PBH merging binaries. Depending on the exact assumptions on the formation of PBH binaries, this translates to stellar-mass range PBHs accounting for a fraction $f_{\text{PBH}} \simeq 3 \times 10^{-3} - 2 \times 10^{-2}$ of the observed dark matter abundance. Such a population of PBHs in combination with hierarchical mergers can best explain the observed LVK events with black hole masses in the range of $\simeq 30 - 45 M_{\odot}$.

I. INTRODUCTION

Since the first detection in 2015 of the merger event of two compact objects [1], the Laser Interferometer Gravitational-wave Observatory (LIGO) [2], in combination with Virgo [3] and the Kamioka Gravitational Wave Detector (KAGRA) [4], have completed three observation runs (O1–O3) [5, 6], while results from the ongoing fourth run (O4) have recently been released in Ref. [7]. The number of binary black holes (BBHs) in the catalog of binary compact object mergers detected by the LIGO-Virgo-KAGRA collaboration (LVK), with a false alarm rate (FAR) of $< 1 \text{ yr}^{-1}$, has reached 153 [7]. Each event in the Gravitational Wave Transient Catalog (GWTC) has an estimate of the primary mass m_1 , secondary mass m_2 , and redshift z , among other quantities. This allows the study of the mass and redshift distributions of the black holes (BHs) that form binaries, giving a merger signal in the gravitational-wave detectors. Moreover, one can use the reported m_1 , m_2 and z information and the LVK reported noise curves to evaluate signal to noise ratios (SNR). Using the reported LVK merger events there are 159 BBHs with an SNR > 8 and $m_2 > 4 M_{\odot}$. We use those events in this analysis.

Previous studies of the LVK data have also discussed the origin of the BBHs, including the possibility that the observations probe multiple populations of BBHs (see e.g. [8–20]). We consider three populations of BBHs: i) binaries following a power-law mass (PL) distribution, as for instance made of first generation BHs (of stellar origin) [21–26], ii) binaries made of BHs resulting from previous mergers, known as hierarchical mergers (HM) [27–34], and iii) binaries made of primordial black holes (PBHs) [35–46].

First generation BHs can be expected to have an approximately power-law mass distribution, starting from a minimum mass of $\simeq 4 M_{\odot}$ with or without a high-mass cut-off, depending on the contribution of population III stars [47, 48]. Such a population of BHs may have a distribution similar to that of their progenitor stars. However, the exact metallicity distribution of the progenitor stars and the environment where these BHs are hosted, may also cause some deviations from a simple power-law on the mass-distribution of the observable by gravitational waves remnant compact objects (see e.g. [24, 49–52]). For stars with a mass larger than $1 M_{\odot}$, including massive enough to form BHs after their collapse, their initial mass follows a power-law distribution of $dN/dM \sim M^{-2.3 \pm 0.7}$ [53]. For simplicity, we will consider such a power-law distribution to model first generation BHs, allowing for the power-law index to be set by the LVK data. Due to the pair-instability mass gap [54], the number of first generation BHs is expected to drop significantly after

* melbouhaddouti@oakland.edu

† cholis@oakland.edu

‡ muhsinaljaf@oakland.edu

some value of mass. For the first generation BHs, starting at $4 M_{\odot}$, we test both a simple power-law mass spectrum, and a mass spectrum described by a power-law with an exponential cutoff at $40M_{\odot}$.

By HM binaries, we refer to the merger of BHs where the most massive member m_1 , is at least a second generation BH. The presence of HM events in the gravitational-wave observations has been discussed as early as 2017 [28, 29], when only two events from the O1 run were publicly available and the O2 run was still ongoing. Using events from runs O1, O2 and O3, Ref. [55] found that at least 10% of GWTC3' s events are HMs, while also [16, 17, 56], found indications for a similar size population of events not originating from first generation BHs. To study the HM population, we rely on the stellar cluster simulations from Ref. [57], from where we model the binaries' primary mass m_1 distribution and the ratio of secondary mass (m_2) to primary mass, $q = m_2/m_1$ distribution.

PBHs [58–60], may have formed in the early Universe from the collapse of density perturbations. In this case, they would contribute to the observed dark matter abundance, even if just as a fraction of it. Furthermore, mergers between such objects can give a detectable signal in gravitational-wave observations [35, 36, 61]. The most direct observable signal from PBHs is that they can contribute to the BBH merger rates and mass spectra measured by the LVK collaboration [7, 56, 62]. Based on the most up to date estimates on the PBH binaries merger rates of Ref. [63], we test if a PBH component can exist in the current LVK BH primary and secondary mass-spectra. This allows us to probe and set constraints on the PBH abundance in the stellar mass range. We derive our results in terms of the fraction of dark matter abundance that is in PBHs $f_{\text{PBH}} = \rho_{\text{PBH}}/\rho_{\text{dm}}$, where ρ_{PBH} is the averaged energy density in PBHs in the Universe and ρ_{dm} is the dark matter energy density of the Universe.

In Section II, we describe the LVK data that we use to study the m_1 , m_2 and redshift z distributions of the observed BBH merges. We also describe the alternative ways in which we model the merger rates from the three populations of BBHs (first generation, HM, and PBH), to account for enough modeling flexibility on each of the three populations. In Section III, we show how these populations of merging BBHs are constrained by the current LVK observations, accounting for the sensitivity of LVK at different frequencies i.e. the observation biases. We find that between 10 and 50 % of all the total merger rate of BBH at low redshifts is of hierarchical origin. Such BH binary mergers can explain the significant population of detected BBHs that contain a BH with a mass of $\geq 30 M_{\odot}$. Moreover, we find that merging PBH binaries in the stellar-mass range are allowed to contribute up to a few % of the total merger rate at $z \leq 1$. Depending on the exact assumptions on the formation of PBH binaries, this translates to a fraction of $f_{\text{PBH}} = 3 \times 10^{-3} - 2 \times 10^{-2}$ on their abundance. Finally, in Section IV, we present our conclusions and discuss how future observations from

ground-based gravitational wave observatories will further inform us on the origins of stellar-mass BHs.

II. METHODOLOGY

We first discuss the LVK observations that we use to study the mass and redshift distributions of the BBHs. We then describe the modeling of the three populations of merging BBHs.

A. The LVK population of black hole binaries

The two LIGO detectors at Hanford Washington and Livingston Louisiana, have a much better sensitivity compared to the Virgo and KAGRA detectors. Still, Virgo and KAGRA allow for an improved localization of the events. For this analysis where we want to use the observed m_1 , m_2 and redshift z -distribution of the BBH mergers in order to probe the underlying populations of these objects, we will rely on the publicly available noise curves for the two LIGO interferometers [64–66].

We use the events from runs O1 to O4a, with m_1 and m_2 central values larger than $4M_{\odot}$ and $\text{SNR} \geq 8$. For each detected event, the LVK collaboration provides the posterior samples on the m_1 and m_2 masses [65, 66]. We use those distributions to make discretized histograms for m_1 and m_2 respectively. Of the 159 events with $m_2 > 4 M_{\odot}$ and $\text{SNR} \geq 8$ there are posterior samples for the 153 BH binaries. We normalize these histograms so that the sum on all bin counts is equal to 1. To obtain our representation of the LVK BBH data, we stack all the m_1 discretized probability density functions (PDFs) to obtain the m_1 distribution, and we stack the m_2 PDFs to obtain the m_2 distribution. These stacked distributions are shown in Fig. 1. Both histograms consist of 15 bins logarithmically spaced between $3M_{\odot}$ and $180M_{\odot}$. Values of masses smaller than $4 M_{\odot}$ appear as the reported LVK posterior samples in [65, 66] extend to these lower masses. To produce the redshift distribution histogram of Fig. 1 for all LVK events, we first take for each binary its relevant redshift posterior distribution. We then stack the redshift posterior distributions from the entire events sample and bin them in 10 linear bins up to $z=1.5$.

In Fig. 2, we show the m_1 vs z distribution of the 153 LVK BBH events that we use in this analysis. The error-bars represent the 90% credible interval reported ranges.

B. Merger rates from first generation black holes

First generation black holes originate from the core collapse of stars. As we briefly discussed in the introduction, stars with a mass large enough to collapse into a BH can be modeled to have a PL mass distribution as the progenitor stars' initial mass does [53]. This justifies testing the

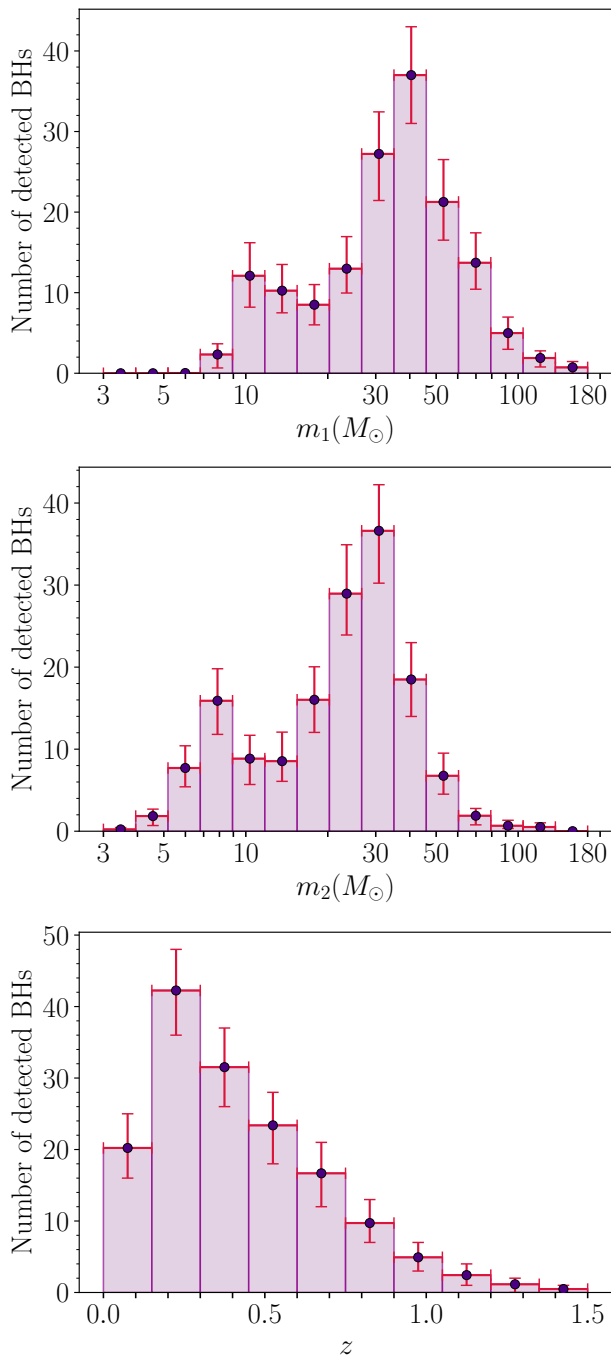


FIG. 1. Histogram of primary mass (top), redshift (middle), and secondary mass (bottom) distribution for BBHs, with Poisson error bars from the GWTC4 events.

mass distribution of BHs detected by LVK using a PL distribution (see also [6]). We note that we do not claim that first generation black holes that form binaries have a mass distribution that strictly follows a PL distribution, just that a PL distribution is a reasonable approximation to the mass distribution of first generation BHs. Following [17], we consider two parameters for this model: α , with $-\alpha$ the exponent of the m_1 distribution, $dN/dm_1 \propto m_1^{-\alpha}$

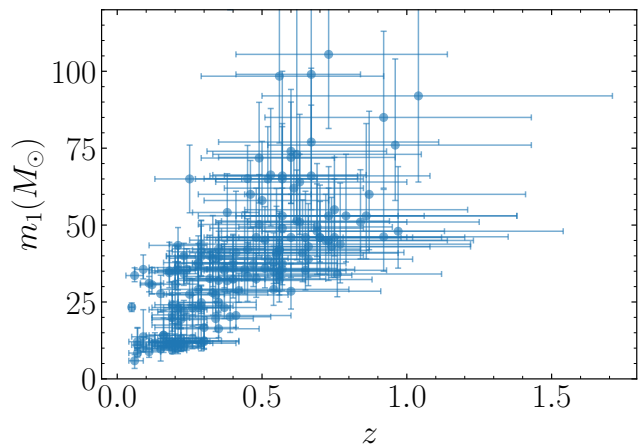


FIG. 2. The primary mass of events from the O1 to O4a LVK runs, as a function of redshift with their 90% credible interval ranges.

and β , the exponent of the ratio $q = m_2/m_1$ distribution ($dN/dq \propto q^\beta$). We fit the values of α and β to the LVK observations.

A better approximation of the mass distribution of first generation BHs is a PL with an exponential cutoff. Such a distribution accounts for the mass distribution of the progenitors of first generation BHs, but also accounts for the pair instability mass gap [54], which results from the progenitor star having a mass large enough to start producing electron positron pairs during the core collapse, which releases enough energy to cause a supernova with no BH formation at the center. The lower end of the mass gap, while still debated, is known to be at least $40M_\odot$ [54]. We choose the exponential cutoff at $40M_\odot$. Thus, the PL with an exponential cutoff mass distribution of m_1 is taken to be,

$$\frac{dN}{dm_1} \propto m_1^{-\alpha} e^{(-m_1/40M_\odot)}. \quad (1)$$

For q we use a simple power-law distribution with an exponent β . We refer to this option as “PLe”.

We test both the PL distribution and the PLe distribution for m_1 and model the redshift distribution for the first generation BH binaries’ comoving merger rate to scale as $R(z) \propto (1+z)^\kappa$ following Refs. [20, 65]. We take $\kappa = 2.7$, which is consistent with the star formation rate [67, 68].

C. Modeling the rates of hierarchical merger binaries

By hierarchical merger binaries HM, we refer to mergers of BH binaries where at least one of the BHs is the result of a previous binary BH merger. We consider the m_1 and q mass distributions from [57], specifically the histograms representing PDFs of higher than first generation BHs in

figures 4 and 6 of Ref. [57]. These histograms are the result of N-body simulations of binary evolution and mergers inside dense stellar clusters. To allow some modeling flexibility for HM binaries, we introduce an additional parameter λ to squeeze or stretch the m_1 distribution. In Fig. 3, we show how different values of λ affect the expected m_1 distribution from HM binaries. In our tests, parameter λ takes values from 0.5 to 1.5 with increments of 0.1.

From Ref. [57], we also adopt the HM binaries' comoving merger rate scaling with redshift as,

$$R_{\text{HM}} \propto \frac{(1+z)^{2.6}}{1 + [(1+z)/(3.2)]^{6.2}}. \quad (2)$$

D. PBH merger rates

PBH binaries can be classified based on their formation time into early binaries and late binaries (for a detailed review, see [44]). Early binaries form before the matter–radiation equality [35, 69]. The evolution of their orbital properties follows two main pathways: (i) unperturbed binaries, which remain outside dark matter halos and just evolve via gravitational-wave emission, and (ii) binaries that stay unperturbed initially, but at some point fall inside halos, where some of them will undergo dynamical effects such as binary–single interactions with other PBH binaries or single PBHs. Instead, late binaries form through dynamical gravitational-wave direct capture of single PBHs inside dark matter halos [36], creating highly eccentric binaries that merge soon after [70]. Thus, the combined total comoving merger rate of PBH binaries at redshift can be written as,

$$R_{\text{total}}(z) = f_{\text{PBH}}^2 \left[R_{\text{captures}}(z) + 2 f_{\text{PBH binaries}} \times (R_{\text{unperturbed}}(z) + R_{\text{binary-single}}(z)) \right], \quad (3)$$

where $R_{\text{unperturbed}}$ is the comoving merger rate from unperturbed early binaries merging outside dark matter halos, $R_{\text{binary-single}}$ is the merger rate of early binaries further evolved through binary–single interactions inside halos, and R_{capture} is the rate of late binaries formed via gravitational-wave induced captures. $f_{\text{PBH binaries}}$ denotes the fraction of PBHs initially bound in binaries. For the allowed PBH merger rate calculation, we take as a starting point $f_{\text{PBH}} = 1$, which is then constrained by the LVK observations.

We use the recent calculations of Refs. [45, 63], where each of these rates has been re-evaluated, and the relevant modeling uncertainties have been quantified. In those works, a large sample of early binaries is simulated forming at $z = 3200$, with their initial semi-major axes and eccentricities (a, e) drawn from the joint PDF evaluated by [35, 39, 69]¹. We take that half of PBHs are in

binaries and track the fraction of dark matter that stays in the intergalactic space, i.e., does not enter the Virial radius of dark matter halos at any time. Our simulations start near the formation of PBH binaries. At this stage, only a small fraction of dark matter is in halos. At $z = 12$, this fraction is just a few percent. However, by today, approximately 90% of all dark matter PBHs are inside halos [72].

PBH binaries that fall inside halos will experience dynamical binary–single interactions that can lead to mergers, hardening, softening, or even ionization (binaries breaking up) [73–76]. Hard binaries become more tightly bound, soft binaries are widened, and sufficiently strong encounters can break a binary [73]. We follow the methodology of Ref. [63] and account for all these effects on the evolution of PBH binaries. The rate of binary–single interactions depends on the local density and dispersion velocity (see also discussion in [45]). For this reason, the merger rates are evaluated for dark matter halos of masses $10^4 - 10^{15} M_{\odot}$, properly tracking the dark matter halo mass function evolution with time. The density of PBHs in each halo follows an NFW profile [77]. In each simulated dark matter halo, the simulations account for the change of density and dispersion velocity with radius and with time within the halo, which affects the environment that the PBH binaries are in (see [45, 63] for further details). All dark matter halos are simulated to grow in mass with time following Ref. [78]. The orbital properties of all binaries inside a halo are tracked through orbit-averaged evolution equations that can lead to hardening all the way to merger, to softening of the binaries, and even to ionizations [63].

Finally, for the late binaries formed inside dark matter halos via gravitational-wave two-body direct captures, their rate of merger is determined using the analytic treatment of [35, 36, 45].

We calculate the comoving merger rate using (3), assuming both monochromatic and lognormal PBH mass distributions. In the monochromatic case, all PBHs have identical source-frame masses $m_1 = m_2 = m_{\text{PBH}}$, while in the lognormal case the mass function is

$$\psi(m) = \frac{1}{\sqrt{2\pi} \sigma m} \exp\left(-\frac{\ln^2(m/m_c)}{2\sigma^2}\right), \quad (4)$$

where m_c denotes the peak mass and $\sigma = 0.6$ is the width of the distribution. In both cases, the characteristic mass (m_{PBH} or m_c) is taken in the range $5M_{\odot} \leq m \leq 80M_{\odot}$.

In Fig. 4 we present the comoving merger rate as a function of redshift z for three representative masses $m_{\text{PBH}} = m_c = 5, 36, \text{ and } 80 M_{\odot}$. Solid lines correspond

unperturbed binaries that remain outside dark matter halos evolve purely via gravitational wave emission following the orbit-averaged Peters equations [71], while binaries that fall into halos are further evolved, including dynamical binary–single interactions (perturbed binaries).

¹ These binaries are evolved to $z = 0$ by combining two approaches:

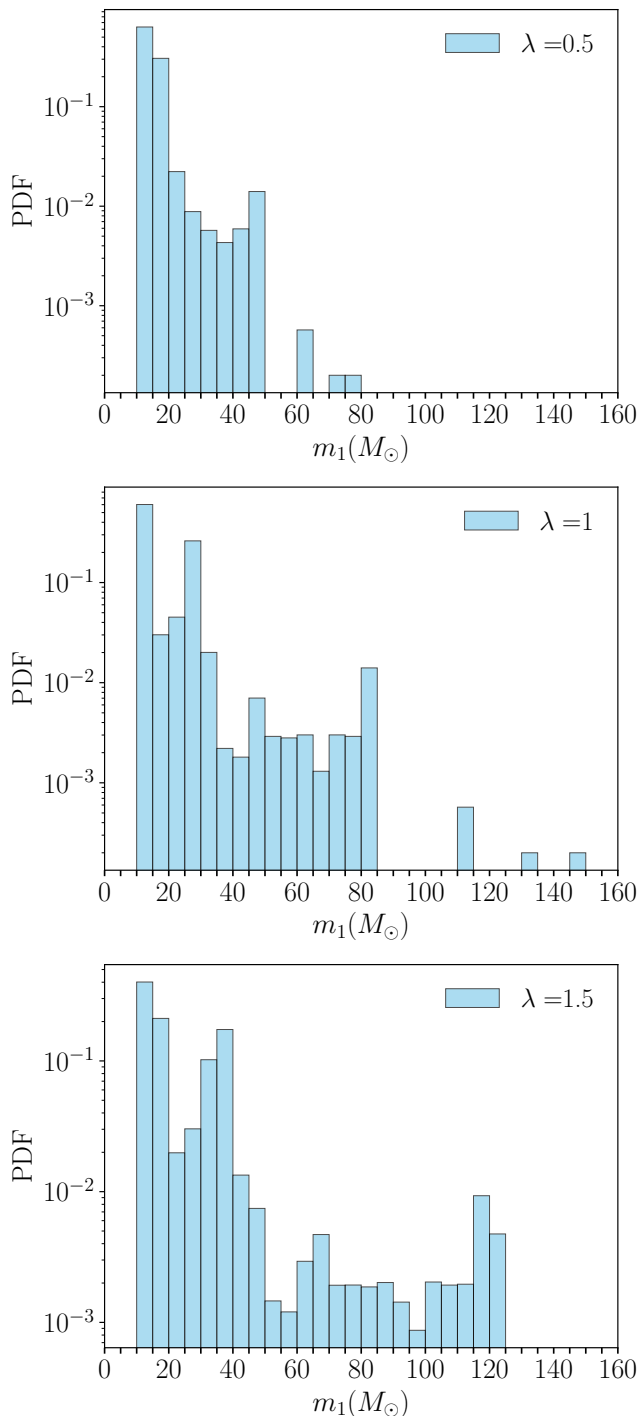


FIG. 3. PDF of primary mass of BHs that are at least second generation BHs. The top histogram is for $\lambda = 0.5$, the middle one for $\lambda = 1$ i.e the PDF obtained from [57], and the bottom histogram is for $\lambda = 1.5$.

to the monochromatic case, while dashed, dot-dashed, and dotted lines correspond to the lognormal distribution. For these calculations we assume $f_{\text{PBH}} = 3 \times 10^{-3}$ and a binary fraction $f_{\text{PBH binaries}} = 0.5$. We find that for the same characteristic mass the lognormal distribution with

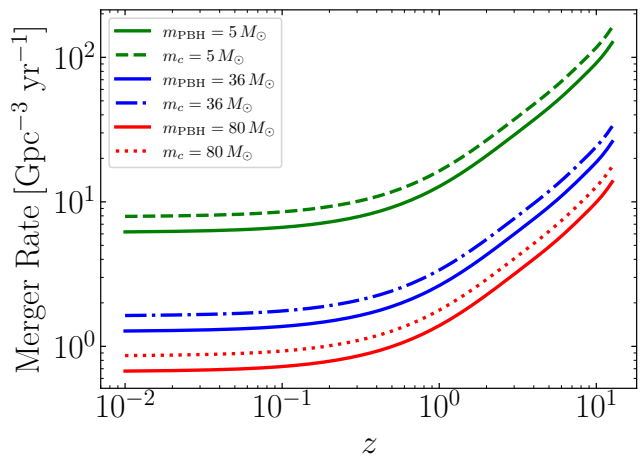


FIG. 4. The comoving merger rate of PBHs binaries as a function of redshift z for monochromatic and for lognormal mass distributions described by Eq.(4) with $\sigma = 0.6$. The rate is calculated as the sum of three merger channels: unperturbed binaries, binary-single interactions within halos, and two body captures using Eq.(3). In all cases, we assume $f_{\text{PBH}} = 3 \times 10^{-3}$ and a binary fraction of $f_{\text{PBH binaries}} = 0.5$.

$\sigma = 0.6$ in Eq. (4) provides slightly higher merger rates.

E. Simulating detectable black hole binary mergers

To simulate BH binaries, we first draw m_1 masses from the considered population; i) first generation BH binaries with a PL distribution for m_1 , ii) first generation BH binaries with a PLe distribution, i.e., PL and an exponential cutoff for m_1 at $40 M_\odot$, iii) HM binaries, or iv) PBH binaries. For each population, we use the relevant q -distribution and then take the product $m_1 \cdot q$ to obtain the m_2 mass. We also assign a redshift value to each simulated BH binary that is consistent with the merger rate dependency on z . In this work, for every merging binary, we also assign a time of arrival of the gravitational waves at Earth. This arrival time is drawn from a uniform distribution that covers the dates the LIGO runs were occurring. This allows us to take into account all the power spectral densities (PSDs) provided by LIGO [65, 66], to correct in our parameter estimation for the fact that the two LIGO sensitivity curves changed with time.

As discussed previously, all reported masses have a measurement error. To account for that in our simulations, we first derive the distribution of m_1 values of the simulated merger events with an $\text{SNR} \geq 8$ for specific model parameters describing the simulated population of BBHs. We then convolve that distribution with a Gaussian function. That Gaussian function has a mass dependent width based on the reported errors on the m_1 and m_2 values of the LVK events, see Refs. [17, 79] for more details. The uncertainty on the m_2 masses is accounted for as the simulated m_2 -distribution is the product of the $m_1 \cdot q$

distribution, where the m_1 -distribution has already been convolved with the Gaussian described above.

To compare our models to the data of Fig. 1, we calculate the SNR for binaries at chosen values of their relevant modeling parameters, e.g., α and β for the PL and the PLe distributions. The choice of PSD depends on the time of gravitational wave arrival at Earth from the simulated binary. We use the PSD that is closest to the simulated gravitational wave arrival time. The SNR equation for each merged BH binary depends on whether one or both LIGO detectors were operational at the time the gravitational waves arrived at Earth. When both LIGO detectors are operational, we use,

$$SNR^2 = \frac{2}{5} \int_{f_{\min}}^{f_{\max}} df \frac{h_c(f)^2}{(2f)^2} \left(\frac{1}{\text{PSD}_H(f)} + \frac{1}{\text{PSD}_L(f)} \right). \quad (5)$$

The indices H and L refer to the Hanford or Livingston detectors respectively, f is the observed gravitational-wave frequency, f_{\min} and f_{\max} are the current range of LIGO's interferometers (taken to be 10 Hz to 4000 Hz), $h_c(f)$ the observed strain amplitude, $\text{PSD}(f) = h_n(f)^2$ ($h_n(f)$ the strain noise amplitude). If only one of the detectors is operational we use instead,

$$SNR^2 = \frac{2}{5} \int_{f_{\min}}^{f_{\max}} df \frac{h_c(f)^2}{\text{PSD}(f) (2f)^2}. \quad (6)$$

The PSD in the above equation is the relevant power spectral density of the operational detector. For a detailed description of h_c and the equations used for the SNR calculation, we refer the reader to [17] and [80].

The total number of simulated merging binaries between redshifts z_1 and z_2 , is obtained using,

$$N_{\text{merger}}(z_1, z_2) = 4\pi \int_{z_1}^{z_2} dz \frac{c \cdot \chi(z)^2 \cdot R_{\text{pop}}(z)}{(1+z)H(z)} \times t_{\text{obs}}, \quad (7)$$

where $\chi(z)$ is the comoving distance, $R_{\text{pop}}(z)$ the comoving merger rate of the considered population, $H(z)$ the Hubble expansion parameter and t_{obs} the duration of the runs O1 to O4a taking into account the duty cycle of each run. By adding all redshift bins, this allows us to generate histograms for m_1 and m_2 of the expected detectable BH binaries from any given modeled population, while also being able to keep track of the redshift distribution of those mergers. We then compare to the histograms of Fig. 1. To minimize the statistical noise on the predicted histograms of m_1 , m_2 and z , we multiply the $R_{\text{pop}}(z)$ by some factor (between 10 and 1000 depending on the population), which we keep track of and properly remove in our reported constraints on the merger rates of the various populations.

F. Best fit parameter estimation with emcee

We use `emcee` [81], to find the best fit parameters of the considered models when comparing to the data. This

involves defining a log-likelihood and a uniform prior distribution for each considered model parameter within the ranges given in Table I.

Model	Parameter	Range
PL	α	[2.5, 4]
	β	[0, 2.5]
	R_{PL}	$[0, 2 \times 10^2] \text{ Gpc}^{-3} \text{ yr}^{-1}$
PL with cutoff (PLe)	α	[2, 4]
	β	[0, 2]
	R_{PLe}	$[0, 2 \times 10^2] \text{ Gpc}^{-3} \text{ yr}^{-1}$
HM	λ	[0.5, 1.5]
	R_{HM}	$[0, 2 \times 10^2] \text{ Gpc}^{-3} \text{ yr}^{-1}$
Mono PBH	m_{PBH}	[5, 80] M_{\odot}
	$f_{\text{PBH, mono}}$	[0, 1]
Lognorm PBH	m_c	[5, 80] M_{\odot}
	$f_{\text{PBH, lognorm}}$	[0, 1]

TABLE I. Range of uniform priors used for each model. PL refers to our simple power-law model for m_1 , PLe to the model that has a power-law with an exponential cutoff for m_1 , HM to hierarchical mergers, Mono PBH to monochromatic PBHs, and Lognorm PBH to PBHs drawn from a lognormal mass-distribution. The reported rates are at $z = 0$ (see text for more details).

We use the representation of the LVK data from Fig. 1. We bin the simulated BBHs from the considered model the same way we bin our data. Since the data represents a number of counts per bin, for the log-likelihood function we use is the Poisson log-likelihood,

$$\ln(\mathcal{L}) = \sum_i k_i \ln(\mu_i) - \mu_i - \ln(k_i!), \quad (8)$$

where i refers to the bin i : $i \leq 15$ refers to the bins of the m_1 histogram, $15 < i \leq 30$ refers to the bins of the m_2 histogram and $30 < i \leq 40$ refers to bins of the z histogram². In Eq. 8, k_i is the number of counts in bin i of the LVK data, while μ_i is the number of counts in bin i of the simulated BBHs from the considered model: $\mu_i = \text{bin counts}(\text{parameters}, i)$. When we test to the data the PL or PLe, their parameters are α , β , i.e. the exponents of the m_1 and q distribution, respectively and also the merger rate R_{PL} (or R_{PLe}). When HMs are considered as an additional population in the fit, the parameter λ is included, which describes the squeezing/stretching

² We recognize that using the Poisson log-likelihood assumes no correlations between neighboring bins. Depending on the exact amplitude of the gravitational-wave signals the posterior PDFs of each event's properties typically span more than one bins in any of the three parameters. Thus a Poisson likelihood is only an approximation.

of the HM m_1 -mass distribution and the merger rates of the HM population R_{HM} . Again, we use flat priors for all our model parameters within the probed volume, shown in Table I. The quoted rates are the comoving rates normalized at $z = 0$.

When running `emcee` to maximize log-likelihood, we use 32 walkers for 50000 iterations, disregarding the first 5000 steps. To get the posterior probabilities, we use the ‘`sampler.get_chain`’ function after using the ‘`sampler.run_mcmc`’ function. We place the walkers initially at $\alpha = 3.5$, $\beta = 1.1$ that is the best fit value from Ref. [56].

The LVK collaboration gives the estimated BBH rate to be $\simeq 20 \text{ Gpc}^{-3} \text{ yr}^{-1}$. In our priors to allow for maximum modeling freedom, we allow for the rates to go as high as $200 \text{ Gpc}^{-3} \text{ yr}^{-1}$. For the HM, we set $\lambda = 1$, which corresponds to the original proposed distribution of Ref. [57], and for the PBHs, our walkers start from $m_{\text{PBH}} = 35$, that was the best fit value from O1-O3 LVK observations [79]. Our walkers have initial values for the normalization of the merger rates at $z = 0$ to be $20 \text{ Gpc}^{-3} \text{ yr}^{-1}$ for each of the PL, the PLe, and the HM populations and $f_{\text{PBH}} = 10^{-3}$ for the PBHs. The normalization rates for the first three populations are chosen to be close to the reported results from Ref. [20], while the initial walkers’ value on f_{PBH} is at the same order of magnitude of Ref. [79]. We have also tested the sensitivity of our final results to the initial position of the walkers. We run `emcee` with random initial/starting positions for our walkers within the ranges of our priors of Table I, with the same number of walkers, steps, and discarded steps as previously described. Our results are practically unaffected by the choice on the starting position of our walkers.

III. RESULTS

In Fig. 5, we show the results of the fit for parameters of α , β , and the associated merger rate of the PL and the PLe models. For the case of the simple power-law model (blue regions, lines and contours) for m_1 , we find α to be $2.84_{-0.10}^{+0.11}$, within 90% credible interval (CI). The central values represent the median value from the posterior PDF. We also find $\beta = 1.11_{-0.89}^{+1.17}$ at 90% CI and the associated comoving merger rate at $z = 0$ to be $R_{\text{PL}} = 117_{-25}^{+37} \text{ Gpc}^{-3} \text{ yr}^{-1}$ at 90% CI. Instead, for the case where the PLe model is tested we find $\alpha = 2.04_{-0.04}^{+0.09}$, $\beta = 1.19_{-0.83}^{+0.74}$ and $R_{\text{PLe}} = 73_{-11}^{+19} \text{ Gpc}^{-3} \text{ yr}^{-1}$ at 90% CI (red regions, lines and contours). We also give these relevant ranges in Table III, for ease of comparison.

While both the PL and PLe are simplified models and we have clear evidence already from the O1-O3 runs for an additional “peak” around 30-40 M_{\odot} in m_1 . Still these models provide a basis to compare with the more complex models of an added HM population or adding both a HM BH population and a PBH population, that we discuss in the following paragraphs. Our results for

the posterior ranges of α and β of the PL model, overlap with the results of Ref. [56], that suggested $\alpha = 3.5_{-0.6}^{+0.6}$ and $\beta = 1.1_{-1.3}^{+1.7}$ for the power-law with a peak model. Furthermore, Ref. [20], using the same sample of BBH observations suggested a broken power-law distribution with an index $\alpha_1 = 1.7_{-1.8}^{+1.2}$ for $m_1 \lesssim 35 M_{\odot}$ and a different index $\alpha_1 = 4.5_{-1.3}^{+1.6}$ for the higher masses. Our PLe model clearly prefers lower values of α than the simple PL model (harder spectrum for m_1). As this model mostly fits the population of BBHs with $m_1 < 40 M_{\odot}$, it is not surprising that our derived range is in agreement with the range of the α_1 index of Ref. [20]. We find that in both the PL and the PLe models the β index is poorly constrained as has been the case also for the LVK collaboration results [20, 56]. There is still a great level of degeneracy between the α and β indices, with a small change in the value of α causing a large change in the values of β . This can be clearly seen in the contours of Fig. 5, for both PL and PLe models³. We note that the small peaks in the posterior PDF of the β parameter more evident in the case of the PLe population are a result of us using the binned data of Fig. 1. However, those peaks are at the 34% CI range. Our results on the merger rates of the PL and PLe population somewhat higher compared to those of Ref. [20], that gets the binary BH merger rate to be between 14 and 26 $\text{Gpc}^{-3} \text{ yr}^{-1}$ at 90% CI. As a note the PLe gives a lower and better constrained merger rate to the PL one. In our fits higher rates are allowed due to the lower values of the β parameter that we find to be still allowed. A smaller value for β allows for many BBHs that would go undetected by LVK. In Appendix A we show results for alternative (wider) priors on β and R_{PL} or R_{PLe} .

To compare between population models we first calculate their Bayesian evidence \mathcal{Z}_A ,

$$\mathcal{Z}_A = \int d\theta_A \mathcal{L}(D|\theta_A) \pi(\theta_A). \quad (9)$$

The index A, here represents the model that we test: i.e. i) PL for the power-law model, ii) PLe for the power-law with exponential cutoff, iii) PL & HM and iv) PLe & HM when considering hierarchical mergers to the PL and the PLe models respectively, v) PL & HM & Mono PBH and vi) PLe & HM & Mono PBH when also adding a population of monochromatic PBHs to models (iii) and (iv) respectively. We also test instead the case where the PBHs follow a lognormal mass distribution as described in Sec. II. Those are cases vii) PL & HM & Lognorm PBH and viii) PLe & HM & Lognorm PBH. The prior distribution on the physical parameters θ_A , are represented as $\pi(\theta_A)$ and are described in Table I.

³ There is a small amount of smoothing in plotting the 2D projection of the posterior PDF that explains why in the β vs R_{PL} panel, for the PLe model the red contours extend marginally beyond the $\beta = 2$ value.

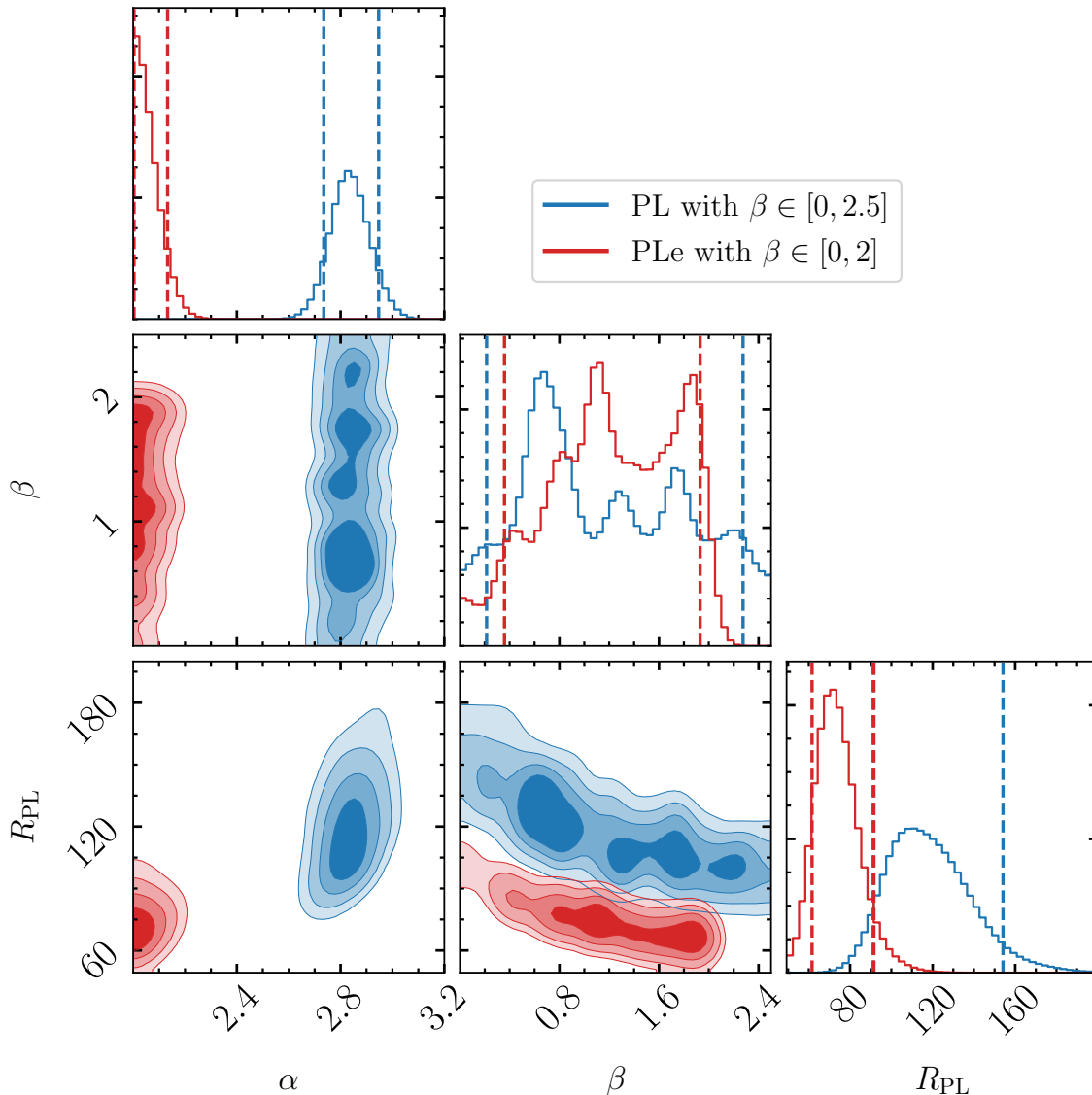


FIG. 5. Corner plot representing the fit parameter values for a simple power-law model (blue lines and contours) and the fit parameter values for a power-law with an exponential cutoff (red lines and contours). The contour lines represent the 34%, 68%, 85% and 95% credible intervals. We also show in the dashed lines the 90% credible interval ranges for each of the parameters values are given in Table III. We universally use the symbol R_{PL} to describe the comoving merger rate parameter in $\text{Gpc}^{-3} \text{yr}^{-1}$ at $z = 0$ (see text for more details).

We use `emcee` to get the likelihood function $\mathcal{L}(D|\theta_A)$ of the data D of Fig. 1, given the parameters θ_A . We present different assumptions on the priors of these models in Appendix A. To obtain the evidence for each model we use version 2.2.1 of `emcee` [81], specifically the ‘`sampler.thermodynamic_integration_log_evidence`’ function after using ‘`PTSampler`’ [82] with a number of temperatures equal to 20, the same number of steps and walkers as described in III F and the number of dimensions corresponding to the model for which the evidence is calculated. It is important to note that we used version 2.2.1 of `emcee` only for the estimation of the evidence for the models we consider in this work. The posterior

samples, likelihoods are obtained with the most recent version of `emcee` available during this work (3.1.6).

The population synthesis models that we test have different number of parameters describing them and thus different prior distributions $\pi(\theta_A)$ expand to wider parameter spaces. Thus, the Bayes factor when comparing model A to B ,

$$\text{BF}_B^A = \frac{Z_A}{Z_B}, \quad (10)$$

formally is not enough to properly compare between the alternative models for the population synthesis of the LVK data D that we test. We can use that criterion to properly compare between models of same complexity

Model	α	β	R_{PL} or R_{PLe}	λ	R_{HM}	m_{PBH} or m_c	f_{PBH} ($\times 10^{-3}$)	$-2\Delta \ln \mathcal{L}$	$\ln \text{BF}$
PL	$2.84^{+0.11}_{-0.10}$	$1.11^{+1.17}_{-0.89}$	117^{+37}_{-25}	-	-	-	-	0	0
PLe	$2.04^{+0.09}_{-0.04}$	$1.19^{+0.74}_{-0.83}$	73^{+19}_{-11}	-	-	-	-	-40	+21
PL & HM	$3.45^{+0.44}_{-0.60}$	$0.76^{+1.49}_{-0.70}$	61^{+52}_{-58}	$1.46^{+0.03}_{-0.43}$	$7.4^{+11.1}_{-1.4}$	-	-	-144	+66
PLe & HM	$2.51^{+0.38}_{-0.35}$	$0.66^{+1.14}_{-0.61}$	54^{+29}_{-23}	$1.48^{+0.02}_{-0.13}$	$5.9^{+2.0}_{-1.2}$	-	-	-150	+71
PL & HM & Mono PBH	$3.54^{+0.41}_{-0.83}$	$0.95^{+1.36}_{-0.88}$	15^{+49}_{-14}	$1.14^{+0.03}_{-0.42}$	$13.2^{+5.7}_{-5.1}$	$38.7^{+3.4}_{-2.3}$	$3.39^{+0.49}_{-0.52}$	-185	+79
PLe & HM & Mono PBH	$2.98^{+0.88}_{-0.75}$	$0.83^{+1.03}_{-0.76}$	21^{+116}_{-19}	$1.15^{+0.01}_{-0.39}$	$14.6^{+4.8}_{-6.4}$	$39.0^{+3.4}_{-2.3}$	$3.35^{+0.50}_{-0.53}$	-186	+80
PL & HM & Lognorm PBH	$3.53^{+0.42}_{-0.92}$	$0.98^{+1.35}_{-0.91}$	$8.4^{+45.6}_{-7.9}$	$1.20^{+0.02}_{-0.66}$	$10.8^{+4.4}_{-5.6}$	$32.7^{+5.5}_{-3.5}$	$6.72^{+0.85}_{-1.18}$	-216	+96
PLe & HM & Lognorm PBH	$2.98^{+0.89}_{-0.56}$	$0.85^{+1.02}_{-0.78}$	23^{+136}_{-22}	$1.20^{+0.02}_{-0.58}$	$11.4^{+4.2}_{-5.6}$	$32.5^{+5.1}_{-3.4}$	$6.76^{+0.83}_{-1.07}$	-216	+97

TABLE II. The fit ranges for the tested models. We present here the results for the prior assumption that $\beta \geq 0$ (we give the results for alternative priors on β and R_{PL} or R_{PLe} in Appendix A). The central values give the median value from the posterior PDF. The upper and lower values define the 90% credible interval range that are also represented in the relevant corner plots as dashed lines. Parameters α , β , λ and f_{PBH} are without units, R_{PL} and R_{HM} are in $\text{Gpc}^{-3}\text{yr}^{-1}$ and m_{PBH} or m_c are in M_{\odot} . The second to last column gives the $-2\Delta \ln \mathcal{L}$ between any population synthesis model “X” and the simple PL model, i.e. Λ_{PL}^X . The last column gives in turn the logarithm of the Bayes factor $\ln \text{BF}_{\text{PL}}^X$ in comparing model “X” to the PL model. In evaluating the range of values on f_{PBH} , we have assumed $f_{\text{PBH}}^{\text{binaries}} = 0.5$.

in the parameters probed as for instance the PL and the PLe for which we use the same prior distributions for the same parameters: α , β and merger rate of the given population evaluated at $z = 0$ and having the same parametric dependence to redshift of $\propto (1+z)^{2.7}$. We can also use the Bayes factor when comparing models (iii) to (iv) i.e. PL or PLe & HM and between models (v), (vi), (vii) and (viii) i.e. PL or PLe & HM & some PBH population.

We report the $\ln \text{BF}_{\text{B}}^{\text{A}} = \ln \mathcal{Z}_{\text{A}} - \ln \mathcal{Z}_{\text{B}}$ and also the likelihood ratio,

$$\Lambda_{\text{B}}^{\text{A}} = -2 \ln \left[\frac{\mathcal{L}_{\text{A}}^{\text{max}}}{\mathcal{L}_{\text{B}}^{\text{max}}} \right] = -2(\ln \mathcal{L}_{\text{A}}^{\text{max}} - \ln \mathcal{L}_{\text{B}}^{\text{max}}), \quad (11)$$

where $\mathcal{L}_{\text{A}}^{\text{max}}$ and $\mathcal{L}_{\text{B}}^{\text{max}}$ are the maximum likelihoods for each model, achieved for their relevant best-fit parameter values. We also refer to this as $-2\Delta \ln \mathcal{L}$.

Comparing PL to PLe models we find a preference for the PLe model by $\ln \text{BF}_{\text{PL}}^{\text{PLe}} = 21$, which is considered a strong evidence in favor of the PLe model (given also in Table II)⁴. We find that the PLe model while it predicts fewer high-mass BBHs it explains better the lower mass end of the LVK observations. Moreover, we find that the preference for a PLe model to a PL even when adding HM or HM and PBHs is persistent as we explain in the following paragraphs. Furthermore, we find a likelihood ratio between PLe and PL to be $\Lambda_{\text{PL}}^{\text{PLe}} = -40$, i.e. in favor of the PLe model (see also Table II).

In Fig. 6, using PL and the PLe populations for the first generation BHs, we add a HM population and probe the five-parameter space (see Table I). We find that the PL and PLe components of these models give the dominant contribution to the LVK mergers but more importantly increase the inferred physical rate, with the PL or PLe merger rates (R_{PL} in the panels of Fig. 6) being up to a factor of 20 higher than the HM merger rates R_{HM} . Adding an HM population allows in our fits for the PL (PLe) populations to adjust better their model parameters to fit the lower LVK masses of Fig. 1. Even for these models as was the case for the simple PL and PLe models, the α parameter for the PLe component has lower (less steep) power-law values of $2.51^{+0.38}_{-0.35}$ compared to the PL component ($3.45^{+0.44}_{-0.60}$). The β parameter for these components is effectively unconstrained but with a preference for $\beta < 1$ which explains also the high values we get for R_{PL} . In Appendix A, we show results with a prior of $-1 \leq \beta$ where the derived ranges of R_{PL} rates can be significantly larger.

A main result from Fig. 6, is also that the λ parameter that describes the stretching of the m_1 HM second generation+ population has a clear preference for $\lambda > 1$ with posterior getting values of $\lambda \simeq 1.5$ which is the end of the probed prior and allows for the HM population to expand to higher masses than originally predicted by Ref. [57]. This may suggest the existence of third and even higher generation BHs in the LVK sample (see e.g. Ref. [83, 84]).

We find that adding a HM component is preferred to a pure PLe model by a Bayes factor $\text{BF}_{\text{PLe}}^{\text{PLe \& HM}} = 50$ and by a likelihood ratio of $\Lambda_{\text{PLe}}^{\text{PLe \& HM}} = -110$. This clear preference for a HM component is also seen when using instead of the PLe model for the first generation BHs the simple PL model. The relevant quantities are

⁴ For each of the population synthesis models, its individual $\ln \mathcal{Z}$ comes with an error. The reported errors from `emcee` on those $\ln \mathcal{Z}$ are $\simeq 5$.

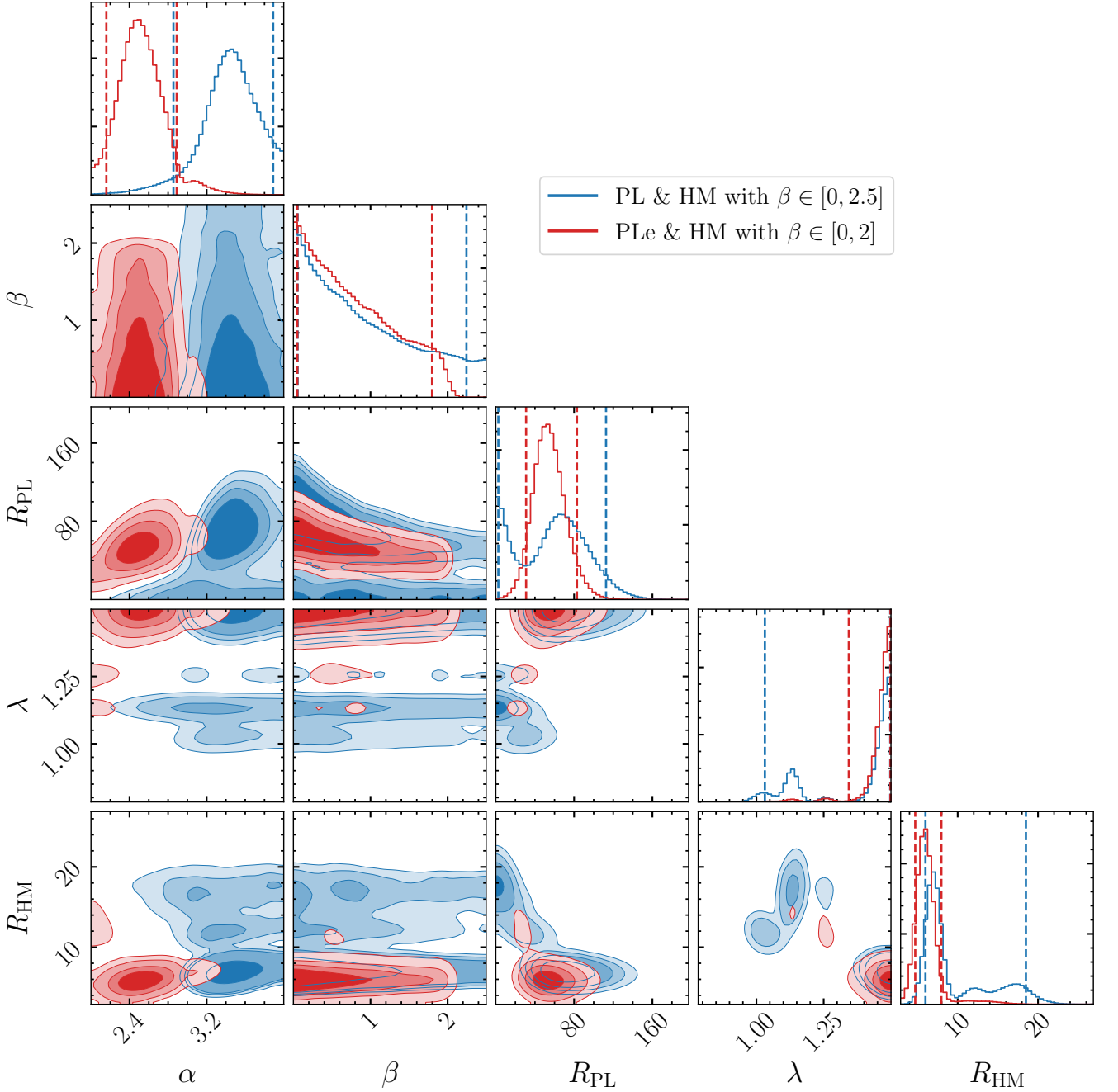


FIG. 6. Similarly to Fig. 5, corner plot representing the fit parameter values for the PL & HM model (blue color) and the PLe & HM model (red color). Contours again represent the 34%, 68%, 85% and 95% CIs and the vertical dashed lines give the 90% CI parameter value ranges. Parameters α , β and λ are without units, while R_{PL} and R_{HM} are in $\text{Gpc}^{-3}\text{yr}^{-1}$.

$\text{BF}_{\text{PL}}^{\text{PL} \& \text{HM}} = 66$ and $\Lambda_{\text{PL}}^{\text{PL} \& \text{HM}} = -144$. The clear evidence for a HM component is due to the significant number of detections of $m_1 \geq 50 M_\odot$, in combination with a few events with $m_2 \geq 40 M_\odot$. In Fig. 7, we show for the PLe & HM population synthesis model a histogram of m_1 and how this HM component explains the high-mass detections. In that figure, while the rate for the PLe component R_{PLe} (blue histogram) is more than 10 times larger than the rate of the HM component R_{HM} , the HM

component (green histogram peaking at $m_1 \simeq 40 M_\odot$) still contributes a little more than half the simulated events. Moreover, we note that while we simulated a power-law with an exponential cut off at $40 M_\odot$ for the first generation BHs, in the detectable sample there are several BHs with $m_1 \geq 50 M_\odot$. This is not from some peculiar choice of α or β for the PLe population (we used in that figure $\alpha = 2.3$ and $\beta = 0.1$). Both the prominent contribution of the HM component and the fact that there

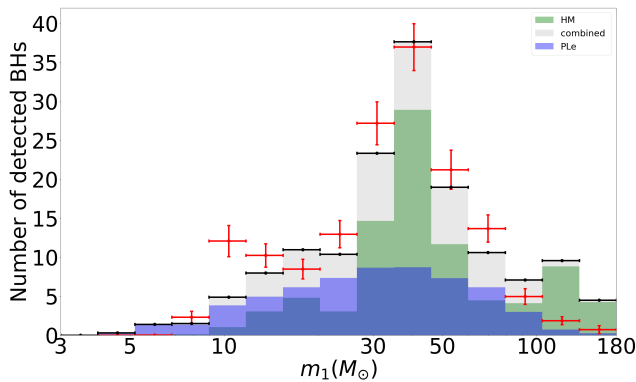


FIG. 7. The m_1 simulated histogram from a PLe & HM population synthesis model. In the blue histogram we show the m_1 BHs from the PLe component, while in the green histogram that clearly peaks at $40 M_\odot$, we show the HM contribution. The combined histogram is given by the gray histogram. The LVK observations are shown by the red (Poisson) error-bars. The comoving merger rate of the PLe component R_{PLe} is more than 10 times larger than the rate of the HM component R_{HM} . However, the populations contribute about the same number of detectable events.

are still several BHs from the PLe component at masses beyond the cut off are a result of LVK’s higher sensitivity on high-mass binaries.

In Fig. 8, for the PLe & HM & Mono PBH population synthesis model, we show the seven-parameter fit ranges. Adding all three components reduces the best-fit merger rates of BBHs from the PLe component while it also allows for a higher best-fit merger rate of BBHs from HMs compared to the simpler PLe & HM model. The PBH component not only improves the fit but also allows for the HM population to better fit the $30 - 50 m_1$ mass range⁵. While there is a preference for $\alpha \simeq 2.8 - 3.4$ and for $\beta \lesssim 1.0$, these two parameters are very weakly constrained. The λ parameter in this model gets values in the $1.15^{+0.01}_{-0.39}$ range in closer agreement to Ref. [57] than what we get for the PLe & HM model. A monochromatic PBH component with a mass in the range of $m_{\text{PBH}} = 39.0^{+3.4}_{-2.3}$ is preferred for $f_{\text{PBH}} = (3.35^{+0.50}_{-0.53}) \times 10^{-3}$ and can help explain the significant number of BBH detections with masses $\sim 40 M_\odot$. Those ranges are also given in Table II.

Comparing the PLe & HM & Mono PBH population synthesis model to the PLe & HM we find a Bayes factor of $\text{BF}_{\text{PLe \& HM \& Mono PBH}}^{\text{PLe \& HM}} = 9$ and a likelihood ratio of $\Lambda_{\text{PLe \& HM}}^{\text{PLe \& HM \& Mono PBH}} = -36$; which suggest a significant improvement in the fit by adding a PBH population. We note that we also tested using a PL distribution instead of a PLe distribution for the first generation black holes. We

get $\text{BF}_{\text{PL \& HM}}^{\text{PL \& HM \& Mono PBH}} = 13$ and a likelihood ratio of $\Lambda_{\text{PL \& HM}}^{\text{PL \& HM \& Mono PBH}} = -41$. The preference for a PBH component is present independently of the existence of an exponential cutoff on the m_1 -distribution. Moreover, the preference for a third component like a PBH component is found as well using our wider priors given in Appendix A. The parameter fit ranges for the PL & HM & Mono PBH and the PL & HM population models are given in Table II. In Figs. 6 and 8, we chose to show the results for the PLe component, as even in these multi-component population models a PLe component for the first generation black holes is somewhat preferred to a PL one. We get $\text{BF}_{\text{PL \& HM}}^{\text{PLe \& HM}} = 4.9$ and $\text{BF}_{\text{PL \& HM \& Mono PBH}}^{\text{PLe \& HM \& Mono PBH}} = 1.5$.

In Fig. 9, we replaced the assumption on the PBH mass-distribution. We show our results on the parameter ranges for the PLe & HM & Lognorm PBH population synthesis model. There is preference for $\alpha \simeq 2.7 - 3.1$ while $\beta \leq 1.5$, but as in the case of Fig. 8, those two parameters are weakly constrained. Subsequently also the merger rate of the PLe component is weakly set to $R_{\text{PL}} = 23^{+136}_{-22}$. The HM component shows a more clear preference for $\lambda \simeq 1.2$ (with $\lambda = 1.20^{+0.02}_{-0.58}$ 90% CI) with a $R_{\text{HM}} = 11.4^{+4.2}_{-5.6}$. The lognormal PBH component is still well constrained to $m_c = 32.5^{+5.1}_{-3.4}$ and $f_{\text{PBH}} = 6.76^{+0.83}_{-1.07}$.

Having a PBH component following a lognormal mass-distribution still has a clear statistical preference compared to not having a PBH component. We get $\text{BF}_{\text{PLe \& HM \& Lognorm PBH}}^{\text{PLe \& HM}} = 26$ and a likelihood ratio of $\Lambda_{\text{PLe \& HM}}^{\text{PLe \& HM \& Lognorm PBH}} = -66$ ⁶. In fact, the lognormal PBH distribution is clearly preferred to the monochromatic distribution by a $\text{BF}_{\text{PLe \& HM \& Mono PBH}}^{\text{PLe \& HM \& Lognorm PBH}} = 17$. Those two models have the same level of free parameters and prior ranges and moreover a lognormal mass-distribution is physically more motivated for PBHs (see Ref. [45] and citations therein for a relevant discussion). The lognormal PBH mass-distribution gives a wider range of masses around the observed peak of $40 M_\odot$ for the m_1 and $30 M_\odot$ for m_2 , in agreement with the representation of the LVK data shown in Fig. 1.

IV. DISCUSSION AND CONCLUSION

In this paper we have analyzed the LVK observations of BBH mergers from the O1 to the O4a observing runs (represented in Figs. 1 and 2), in order to assess the origin of these merging binaries. We use `emcee` [81], to test and maximize the log-likelihood of a given model with parameters within prior ranges, given the LVK observations (see Section II F and Table I).

We test a sequence of population synthesis hypotheses. 1) that these these binaries are just first generation black

⁵ We remind the reader that we account for mass resolution uncertainties in the LVK data as described in Section II E, thus even a monochromatic PBH mass-distribution contributes in more than one mass-bin.

⁶ When using instead the PL assumption for the first generation black holes we get $\text{BF}_{\text{PL \& HM \& Lognorm PBH}}^{\text{PL \& HM}} = 30$ and a likelihood ratio of $\Lambda_{\text{PL \& HM}}^{\text{PL \& HM \& Lognorm PBH}} = -72$.

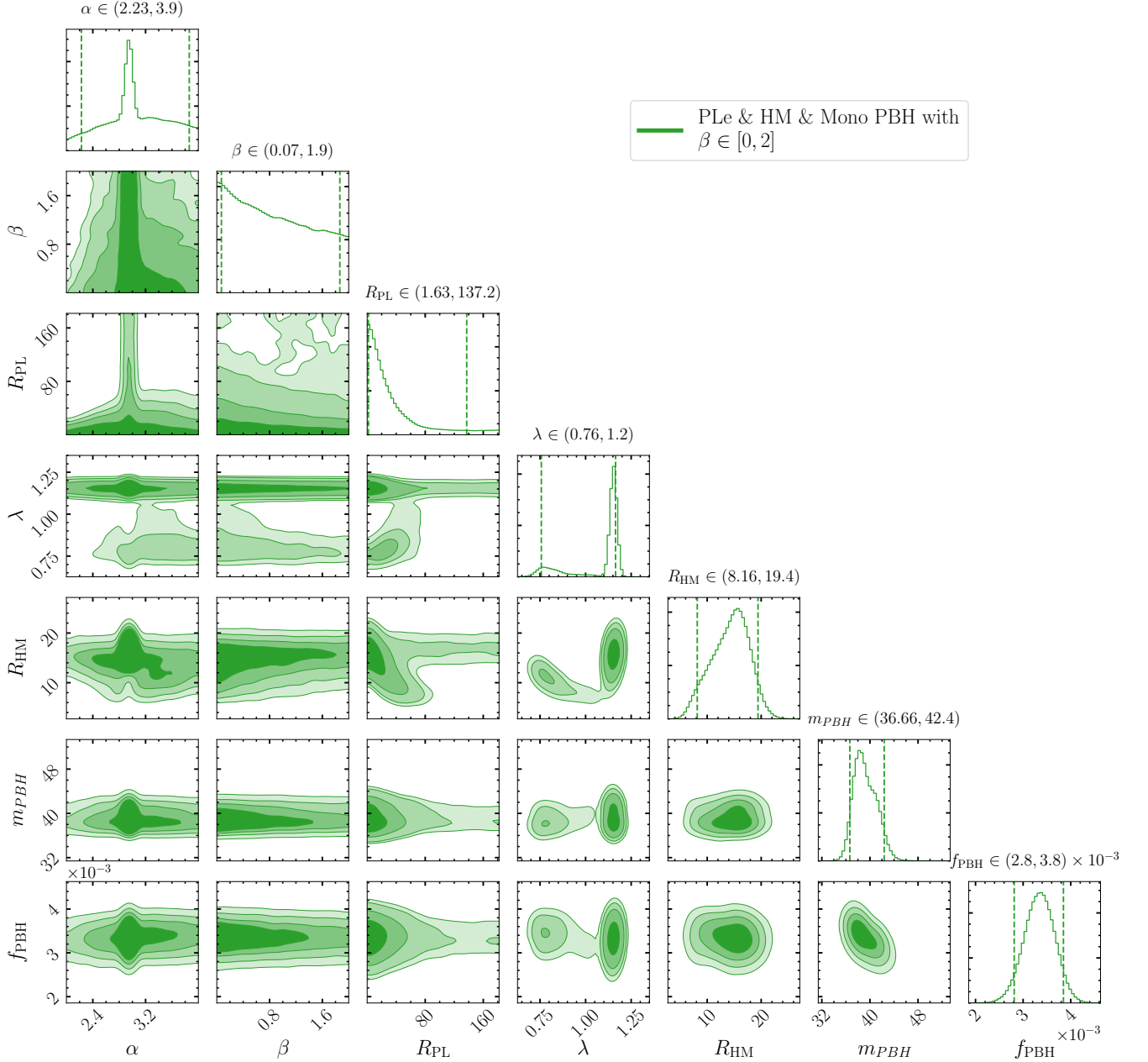


FIG. 8. Corner plot representing the fit parameter ranges for a population synthesis models that includes PLe & HM & monochromatic PBHs. m_{PBH} is in M_{\odot} , while f_{PBH} is unitless. In evaluating the range of values on f_{PBH} , we have assumed $f_{PBH \text{ binaries}} = 0.5$.

holes following a power-law mass distribution without or with an exponential cutoff in their primary mass (PL and PLe model respectively). 2) that in addition to that PL or PLe populations there is a component of hierarchical BH mergers (we refer to is as HM) possibly taking place in dense stellar environments. We use as a base model for that HM population the simulation work of Ref. [57], allowing for some degree of freedom in the predicted mass distribution of the second generation or higher BH masses (see Fig. 3). We refer to these population synthesis models as PL & HM or PLe & HM. 3) that in addition to the PL or

PLe and the HM populations there is a third component of PBH merging binaries in the LVK observations. For that third component we test and derive limits for both the case that the PBH mass-distribution is monochromatic and the case that it arises from a lognormal distribution. For the PBH merger rates we rely on the latest estimates of Ref. [63] (see also Fig. 4).

Comparing the PL and PLe models to the LVK observations we find results similar to earlier works from the O1-O3 observations, i.e. a power-law index $\alpha \simeq 2 - 3$ with a mostly positive index β for the distribution of the

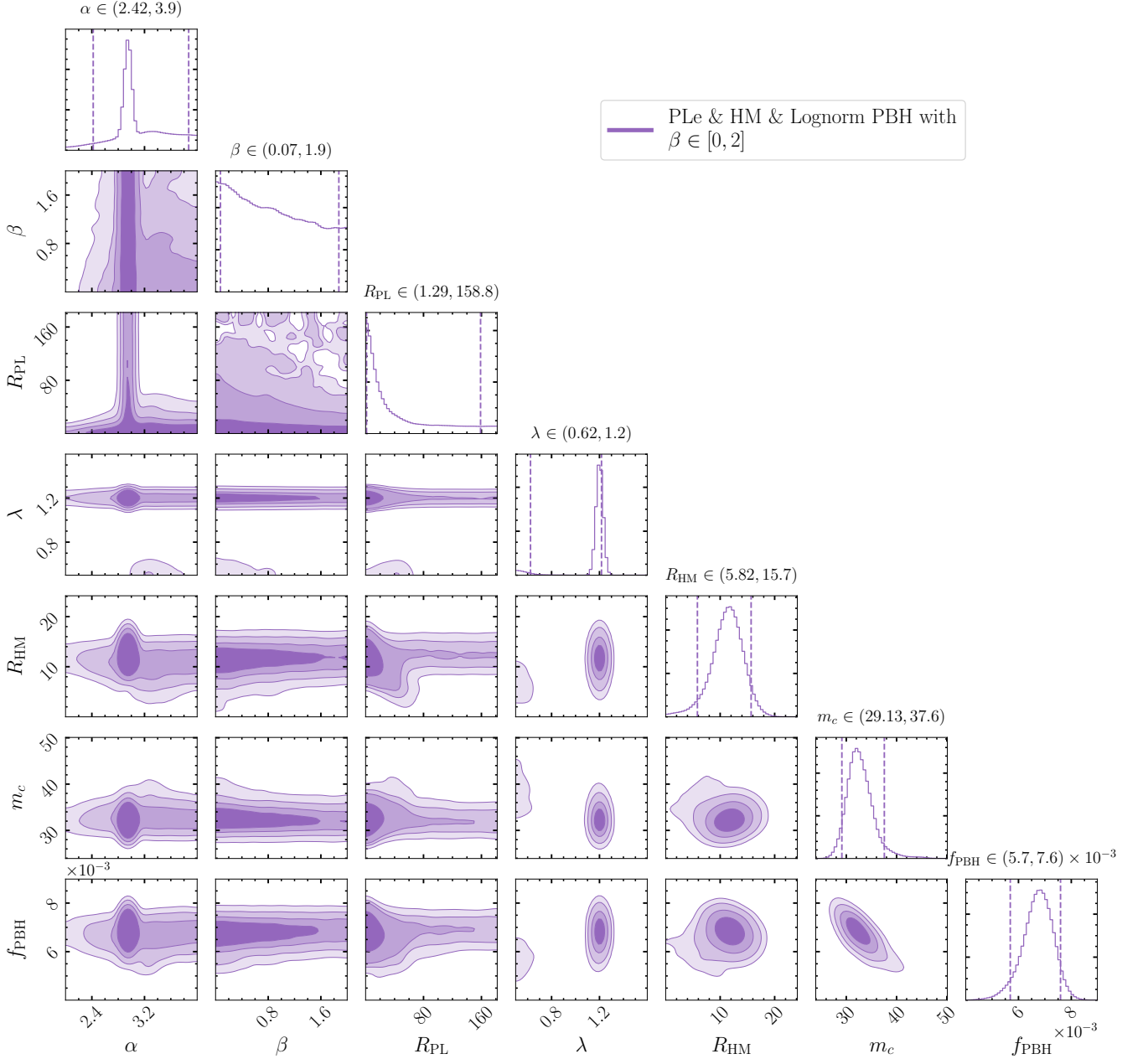


FIG. 9. Corner plot similar to Fig. 8, but for the PLe & HM & Lognorm PBH population synthesis model. Again, in evaluating the range of values on f_{PBH} , we have assumed $f_{\text{PBH binaries}} = 0.5$.

BBH m_2/m_1 ratio (see detailed discussion in Section II). Depending on the exact prior assumptions on the range of α and β , the first generation BHs without any additional component of BBHs have a rate that is $R_{\text{PL}} \simeq 5 - 100 \text{ Gpc}^{-3}\text{yr}^{-1}$ (Figs. 5 and 12).

However, we find that the LVK observations strongly prefer a HM population in addition to the PL or PLe BBH population. We find that even more than half of the observed BBHs may be associated to the HM population (see Fig. 7), with a rate for that population to be $R_{\text{HM}} \simeq 5 - 20 \text{ Gpc}^{-3}\text{yr}^{-1}$. That can also reduce the rate of R_{PL} to as low as $\sim 10 \text{ Gpc}^{-3}\text{yr}^{-1}$ but in

fact given the freedom in the other modeling parameters it makes the PL or PLe rates and the index β mostly unconstrained as we show in Figs. 6, 13 and in Tables II and III. Furthermore, our fits indicate the need for a HM population that contains BHs that may even be third generation. To best-fit the observations we had to deform the mass-distribution of Ref. [57], in such a manner as to increase the masses of the black holes from HMs. Works as in Refs [33, 55, 83, 84], have also come to a similar conclusion. Whether a dominant HM population is indeed detected in gravitational waves, will be resolved by the continuing LVK and future observations. We leave such

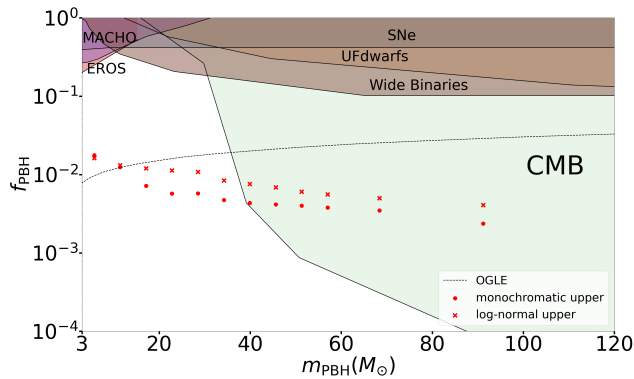


FIG. 10. The 95% upper limits on the PBH abundance f_{PBH} vs the PBH mass m_{PBH} . In the dots we show the limits for a monochromatic mass-distribution, while with the “x” symbols the limits for a lognormal distribution with $m_c = m_{\text{PBH}}$. We assume $f_{\text{PBH binaries}} = 0.5$. We provide for comparison upper limits from other probes on PBHs.

a question for future work.

Finally, we find that a small population of merging PBH binaries is favored to just the PL & HM or the PLe & HM synthesis models. Adding the PBH population improves the likelihood by $2\Delta\ln\mathcal{L}$ by 30 – 60 and gives a Bayes factor of at least $\ln\text{BF} = 15$ in favor of that third component to the observed BBHs (see Tables II and III, and the text in Section III). This result has been reached with alternative prior assumptions. Whether from a monochromatic or a lognormal mass distribution, adding a PBH population helps better explain in the LVK observations the prominent peaks at $m_1 \sim 40 M_\odot$ and $m_2 \sim 30 M_\odot$ but also their redshift distribution. If such a population exists its preferred mass range is $\simeq 30 - 40 M_\odot$ with the PBHs accounting for a fraction $f_{\text{PBH}} \simeq 3 - 8 \times 10^{-3}$ of the observed dark matter abundance in the Universe (see Figs. 8, 9 and 14). In Fig. 10, we present the updated limits on PBH abundance for masses between 5 and $80 M_\odot$. The LVK limits are most competitive for masses in the range of $5 - 40 M_\odot$. We show other limits from Refs. [85–95]. The OGLE limits are depicted with a dashed line given their significant systematics (see Ref. [96]).

In the corner plots of Figs. 8, 9 and 14, and in Fig. 10 and in we assumed that half the PBHs are in binaries ($f_{\text{PBH binaries}} = 0.5$) which is closer to the typical assumption when comparing the gravitational-wave limits on PBHs to other probes. However, for an $f_{\text{PBH}} \simeq 1 \times 10^{-2}$ the fraction of PBHs in binaries is smaller than 0.5. In Fig. 11, we show the 95% upper limits on f_{PBH} as a function of monochromatic PBH mass evaluated for several values on $f_{\text{PBH binaries}}$ of 0.03, 0.05, 0.1, and 0.5. Those values allow us to account for some level of uncertainty on the PBH binary population. Furthermore Ref. [39], has provided a scaling between f_{PBH} and $f_{\text{PBH binaries}}$ (see their Fig. 1). Accounting for that scaling, a more realistic limit on f_{PBH} with m_{PBH} is provided for the lines with $f_{\text{PBH binaries}}$ 0.03-0.05, i.e. the range between the

blue solid line and the orange dashed line. Thus for $m_{\text{PBH}} \simeq 30 - 40 M_\odot$, $f_{\text{PBH}} \sim 2 \times 10^{-2}$.

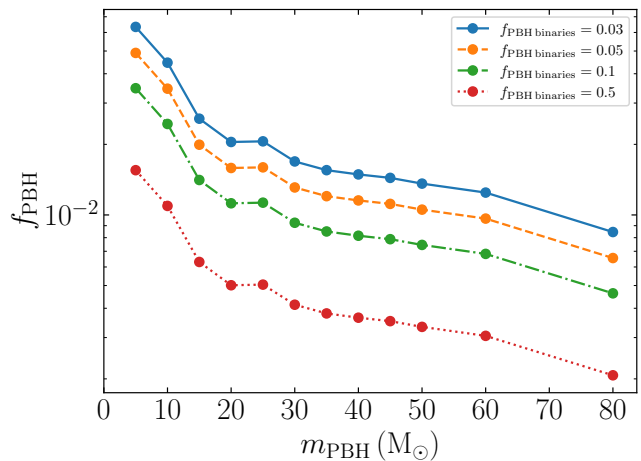


FIG. 11. The 95% upper limits on f_{PBH} as function of monochromatic PBH mass. These limits are obtained by fixing PBH binary fraction $f_{\text{PBH binaries}}$ at 0.03, 0.05, 0.1 and 0.5. We observe that as we increase the value of $f_{\text{PBH binaries}}$, a significant suppression occurs in f_{PBH} .

Future observations from ground-based gravitational-wave interferometers will allow us to further explore the properties of the population of first generation BHs, the contribution of hierarchical mergers as well as the potential contribution of PBHs in the observed BBH population. Including the spin of the observed black holes will also become an important tool in that endeavor (see for instance Ref [97]). In particular since PBHs even in the most dense dark matter halos do not give hierarchical mergers of their own, if they come with a narrow mass range they would only contribute to the m_1 and m_2 mass spectra but have smaller typical values of spins compared to the HM population. Furthermore, the PBH comoving merger rates do increase with increasing redshift even to redshifts $z \sim 20$, when instead any HM population that requires time for this process to occur, could not have been prominent at too high redshifts.

ACKNOWLEDGMENTS

The authors would like to thank David Garfinkle, Iason Krommydas and Yi-Ming Zhong for valuable discussions. MEB, MA and IC are supported by the National Science Foundation, under grant PHY-2207912.

This research has made use of data or software obtained from the Gravitational Wave Open Science Center (gwosc.org), a service of the LIGO Scientific Collaboration, the Virgo Collaboration, and KAGRA. This material is based upon work supported by NSF’s LIGO Laboratory which is a major facility fully funded by the National Science Foundation, as well as the Science and Technology Facilities Council (STFC) of the United Kingdom, the

Max-Planck-Society (MPS), and the State of Niedersachsen/Germany for support of the construction of Advanced LIGO and construction and operation of the GEO600 detector. Additional support for Advanced LIGO was provided by the Australian Research Council. Virgo is funded, through the European Gravitational Observatory (EGO), by the French Centre National de Recherche Scientifique (CNRS), the Italian Istituto Nazionale di Fisica Nucleare (INFN) and the Dutch Nikhef, with contributions by institutions from Belgium, Germany, Greece, Hungary, Ireland, Japan, Monaco, Poland, Portugal, Spain. KAGRA is supported by Ministry of Education, Culture, Sports, Science and Technology (MEXT), Japan Society for the Promotion of Science (JSPS) in Japan; National Research Foundation (NRF) and Ministry of Science and ICT (MSIT) in Korea; Academia Sinica (AS) and National Science and Technology Council (NSTC) in Taiwan.

Appendix A: Testing alternative assumptions on the prior-ranges of models

In the main text we used flat priors in the ranges described by Table I. Here we show results assuming $-1 \leq \beta$. Our main results are summarized in Table III and can be directly compared to the results of Table II.

We find that for the simple PL and PLe population synthesis models the posterior PDFs and the 90% CI ranges of α are essentially the same (the upper and lower values defining them change within a few % between the $-1 \leq \beta$ and the $0 \leq \beta$ priors)⁷. Also, the results for R_{PL} are similar, though spanning a somewhat less constrained range; while the result for the upper end of the β range are roughly the same as well. In Fig. 12, show for the PL and the PLe populations our equivalent results to those presented in Fig. 5 of the main text.

For the PL & HM and the PLe & HM our fit results are shown in Fig. 13. The alternative choice for the β

priors has a marginal effect on the contour ranges and the 90% CIs (changes of $O(10\%)$ of the values that define the range of the CIs) for α , λ and the R_{HM} . Changing the prior range for the β index only affects its posterior range and importantly the R_{PL} range. Allowing the β parameter to be negative, lets the merger rates of the PL and PLe components to take larger values. This is expected. As we described in the main text, negative values of β allow for many BBHs in the Universe with low values of mass ratios, many of which would go undetected.

In Fig. 14, we show our fit results for the PLe & HM & Mono PBH population model (top panel) and for the PLe & HM & Lognorm PBH model (bottom panel). Our results for the PBH properties, i.e their mass-distribution and their abundance f_{PBH} are essentially the same to those from the main text. Also, the ranges for the index α the the HM population's λ parameter and their merger rates R_{HM} are very similar to the results given in Table II and Figs. 8 and 9. Again the main effect of increasing the range of the prior distribution of β is to expand its posterior distribution to lower values as well and to increase somewhat the 90% CI ranges for rate R_{PL} .

Finally, for our tests with the $-1 \leq \beta$ priors, we find very similar differences in the log-likelihoods $-2\Delta\ln\mathcal{L}$ and also in the evidence values for these populations and subsequently the Bayes factors when comparing between alternative population synthesis models. The statements made in the main text regarding the preference for a HM population to a simple PL or a PLe model and further statistical preference for an additional PBH component to the PL & HM or the PLe & HM models remain true. In fact, in Table IV, we show results where we let R_{PL} and R_{PLe} to take as high values as $2 \times 10^3 \text{ Gpc}^{-3} \text{ yr}^{-1}$. Even for that extremely free set of priors for the PL and PLe rates there still is preference for a HM and a PBH population with effectively the same values on their model parameters.

-
- [1] B. P. Abbott *et al.* (LIGO Scientific Collaboration and Virgo Collaboration), “Observation of gravitational waves from a binary black hole merger,” *Phys. Rev. Lett.* **116**, 061102 (2016).
 - [2] J. Aasi *et al.* (LIGO Collaboration), “Advanced LIGO,” *Classical and Quantum Gravity* **32**, 074001 (2015), [arXiv:1411.4547 \[gr-qc\]](https://arxiv.org/abs/1411.4547).
 - [3] T. Accadia *et al.*, “Virgo: a laser interferometer to detect gravitational waves,” *Journal of Instrumentation* **7**, P03012 (2012).
 - [4] T. Akutsu *et al.* (KAGRA), “Overview of KAGRA: Detector design and construction history,” *PTEP* **2021**, 05A101 (2021), [arXiv:2005.05574 \[physics.ins-det\]](https://arxiv.org/abs/2005.05574).

- [5] B. P. Abbott *et al.* (LIGO Scientific Collaboration and Virgo Collaboration), “Gwct-1: A gravitational-wave transient catalog of compact binary mergers observed by ligo and virgo during the first and second observing runs,” *Phys. Rev. X* **9**, 031040 (2019).
- [6] R. Abbott *et al.* (LIGO Scientific Collaboration, Virgo Collaboration, and KAGRA Collaboration), “Population of merging compact binaries inferred using gravitational waves through gwct-3,” *Phys. Rev. X* **13**, 011048 (2023).
- [7] A. G. Abac *et al.* (LIGO Scientific, VIRGO, KAGRA), “GWTC-4.0: Updating the Gravitational-Wave Transient Catalog with Observations from the First Part of the Fourth LIGO-Virgo-KAGRA Observing Run,” (2025), [arXiv:2508.18082 \[gr-qc\]](https://arxiv.org/abs/2508.18082).
- [8] Gert Hütsi, Martti Raidal, Ville Vaskonen, and Hardi Veermäe, “Two populations of LIGO-Virgo black holes,” *JCAP* **03**, 068 (2021), [arXiv:2012.02786 \[astro-ph.CO\]](https://arxiv.org/abs/2012.02786).
- [9] Ken K. Y. Ng, Salvatore Vitale, Will M. Farr, and Carl L.

⁷ We remind the reader that for the PL model we used $\beta \leq 2.5$ and for the PLe $\beta \leq 2$.

Model	α	β	R_{PL} or R_{PLe}	λ	R_{HM}	m_{PBH} or m_c	f_{PBH} ($\times 10^{-3}$)	$-2\Delta \ln \mathcal{L}$	$\ln \text{BF}$
PL	$2.80^{+0.15}_{-0.11}$	$0.83^{+1.45}_{-1.11}$	121^{+78}_{-29}	-	-	-	-	0	0
PLe	$2.04^{+0.09}_{-0.04}$	$1.19^{+0.74}_{-0.90}$	73^{+21}_{-11}	-	-	-	-	-40	+21
PL & HM	$3.43^{+0.46}_{-0.69}$	$-0.08^{+2.05}_{-0.85}$	77^{+104}_{-74}	$1.45^{+0.05}_{-0.14}$	$7.7^{+11.5}_{-1.6}$	-	-	-141	+66
PLe & HM	$2.49^{+0.39}_{-0.33}$	$-0.06^{+1.66}_{-0.63}$	74^{+92}_{-37}	$1.48^{+0.02}_{-0.07}$	$5.9^{+1.5}_{-1.2}$	-	-	-151	+71
PL & HM & Mono PBH	$3.54^{+0.41}_{-0.84}$	$-0.30^{+2.33}_{-0.66}$	39^{+126}_{-37}	$0.85^{+0.31}_{-0.14}$	$12.2^{+5.9}_{-4.4}$	$38.5^{+3.3}_{-2.2}$	$3.41^{+0.48}_{-0.53}$	-185	+79
PLe & HM & Mono PBH	$2.99^{+0.89}_{-0.82}$	$-0.25^{+1.94}_{-0.70}$	40^{+118}_{-36}	$1.15^{+0.01}_{-0.40}$	$14.4^{+4.8}_{-6.3}$	$38.9^{+3.4}_{-2.2}$	$3.35^{+0.51}_{-0.53}$	-186	+81
PL & HM & Lognorm PBH	$3.52^{+0.43}_{-0.99}$	$-0.42^{+2.48}_{-0.56}$	24^{+137}_{-23}	$1.19^{+0.02}_{-0.67}$	$10.7^{+4.3}_{-6.3}$	$32.8^{+6.0}_{-3.6}$	$6.67^{+0.87}_{-1.24}$	-216	+96
PLe & HM & Lognorm PBH	$3.04^{+0.86}_{-0.69}$	$-0.30^{+2.00}_{-0.66}$	42^{+121}_{-40}	$1.20^{+0.02}_{-0.63}$	$11.2^{+4.4}_{-5.6}$	$32.6^{+4.6}_{-3.4}$	$6.72^{+0.83}_{-0.99}$	-216	+97

TABLE III. The fit ranges for the tested models. We present here the results for the prior assumption that $\beta \in [-1, 2]$ (we give the results for the alternative prior on β in Appendix A). The central values give the median value from the posterior PDF. The upper and lower give the 90% credible interval range that are also represented in the relevant corner plots as dashed lines. Parameters α , β , λ and f_{PBH} are without units, R_{PL} and R_{HM} are in $\text{Gpc}^{-3}\text{yr}^{-1}$ and m_{PBH} or m_c are in M_{\odot} . The second to last column gives the $-2\Delta \ln \mathcal{L}$ between any population synthesis model “X” and the simple PL model, i.e. $\Lambda_{\text{PL}}^{\text{X}}$. The last column gives in turn the logarithm of the Bayes factor $\ln \text{BF}_{\text{PL}}^{\text{X}}$ in comparing model “X” to the PL model.

Model	α	β	R_{PL} or R_{PLe}	λ	R_{HM}	m_{PBH} or m_c	f_{PBH} ($\times 10^{-3}$)	$-2\Delta \ln \mathcal{L}$
PL	$2.84^{+0.11}_{-0.10}$	$1.11^{+1.17}_{-0.89}$	117^{+37}_{-25}	-	-	-	-	0
PLe	$2.04^{+0.09}_{-0.04}$	$1.19^{+0.74}_{-0.83}$	73^{+19}_{-11}	-	-	-	-	-40
PL & HM	$3.46^{+0.43}_{-0.51}$	$0.79^{+1.44}_{-0.73}$	63^{+50}_{-59}	$1.46^{+0.03}_{-0.44}$	$7.3^{+10.8}_{-1.3}$	-	-	-140
PLe & HM	$2.51^{+0.38}_{-0.34}$	$0.66^{+1.15}_{-0.61}$	54^{+29}_{-24}	$1.48^{+0.02}_{-0.19}$	$5.9^{+2.4}_{-1.2}$	-	-	-150
PL & HM & Mono PBH	$3.53^{+0.43}_{-0.86}$	$0.95^{+1.36}_{-0.87}$	15^{+48}_{-14}	$1.14^{+0.02}_{-0.42}$	$13.4^{+5.4}_{-5.3}$	$38.7^{+3.5}_{-2.2}$	$3.38^{+0.50}_{-0.52}$	-185
PLe & HM & Mono PBH	$2.96^{+0.75}_{-0.40}$	$0.93^{+0.96}_{-0.85}$	412^{+1261}_{-406}	$1.15^{+0.01}_{-0.41}$	$15.7^{+4.4}_{-7.3}$	$38.8^{+3.5}_{-2.2}$	$3.37^{+0.50}_{-0.55}$	-186
PL & HM & Lognorm PBH	$3.53^{+0.42}_{-0.92}$	$0.99^{+1.34}_{-0.91}$	$8.4^{+47.7}_{-8.0}$	$1.19^{+0.02}_{-0.67}$	$10.8^{+4.4}_{-6.3}$	$32.7^{+5.2}_{-3.5}$	$6.70^{+0.85}_{-1.16}$	-216
PLe & HM & Lognorm PBH	$2.96^{+0.65}_{-0.06}$	$0.98^{+0.92}_{-0.88}$	692^{+1013}_{-686}	$1.20^{+0.02}_{-0.63}$	$12.0^{+4.2}_{-5.7}$	$32.3^{+5.0}_{-3.3}$	$6.83^{+0.81}_{-1.06}$	-216

TABLE IV. The fit ranges for the tested models. We present here the results for the prior assumption that $0 \leq \beta$ with R_{PL} and $R_{\text{PLe}} \leq 2 \times 10^3 \text{Gpc}^{-3}\text{yr}^{-1}$. As in Table II, the central values give the median value from the posterior PDF of each parameter. The upper and lower give the 90% credible interval range that are also represented in the relevant corner plots as dashed lines. The last column gives the $-2\Delta \ln \mathcal{L}$ between any population synthesis model “X” and the simple PL model. While the rates R_{PL} and R_{PLe} span much greater ranges, compared to the results of the main text, our results for the HM and the PBH components properties and statistical significance are effectively unchanged.

- Rodriguez, “Probing multiple populations of compact binaries with third-generation gravitational-wave detectors,” *Astrophys. J. Lett.* **913**, L5 (2021), arXiv:2012.09876 [astro-ph.CO].
- [10] Vaibhav Tiwari, “Exploring Features in the Binary Black Hole Population,” *Astrophys. J.* **928**, 155 (2022), arXiv:2111.13991 [astro-ph.HE].
- [11] V. De Luca, G. Franciolini, P. Pani, and A. Riotto, “Bayesian Evidence for Both Astrophysical and Primordial Black Holes: Mapping the GWTC-2 Catalog to Third-Generation Detectors,” *JCAP* **05**, 003 (2021), arXiv:2102.03809 [astro-ph.CO].
- [12] Gabriele Franciolini, Vishal Baibhav, Valerio De Luca, Ken K. Y. Ng, Kaze W. K. Wong, Emanuele Berti, Paolo Pani, Antonio Riotto, and Salvatore Vitale, “Searching for a subpopulation of primordial black holes in LIGO-Virgo gravitational-wave data,” *Phys. Rev. D* **105**, 083526 (2022), arXiv:2105.03349 [gr-qc].
- [13] Christos Karathanasis, Suvodip Mukherjee, and Simone Mastrogiovanni, “Binary black holes population and cosmology in new lights: signature of PISN mass and formation channel in GWTC-3,” *Mon. Not. Roy. Astron. Soc.* **523**, 4539–4555 (2023), arXiv:2204.13495 [astro-ph.CO].
- [14] Lang Liu, Zhi-Qiang You, You Wu, and Zu-Cheng Chen, “Constraining the merger history of primordial-black-hole binaries from GWTC-3,” *Phys. Rev. D* **107**, 063035 (2023), arXiv:2210.16094 [astro-ph.CO].
- [15] Hye-Jin Park, Shin-Jeong Kim, Shinna Kim, and Maurice H. P. M. van Putten, “On the Mass Function of GWTC-2 Binary Black Hole Systems and Their Progenitors,”

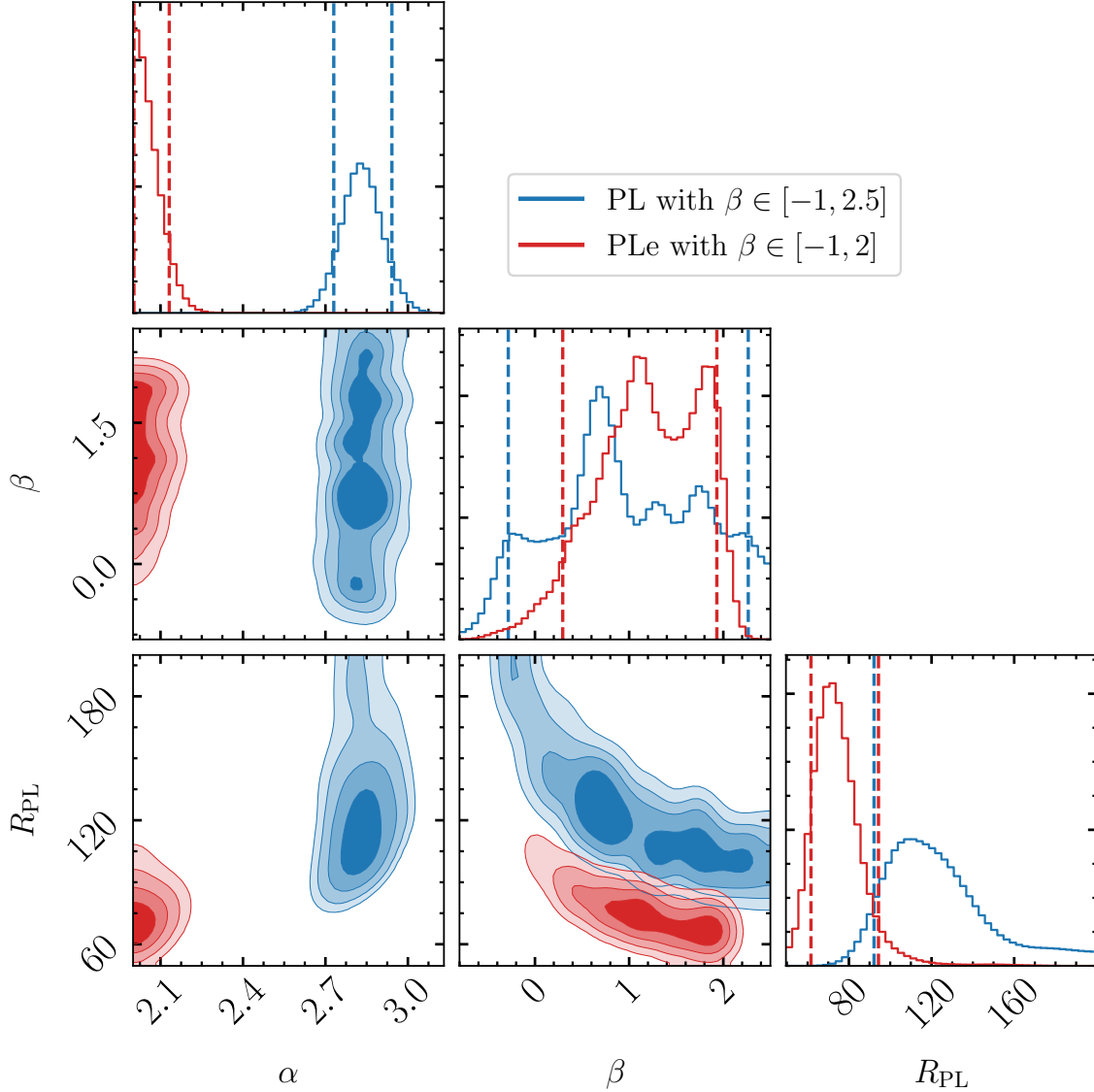


FIG. 12. Corner plot similar to that of Fig. 5, but with prior assumption on $-1 \leq \beta$.

- Astrophys. J.* **938**, 69 (2022), arXiv:2211.07584 [astro-ph.HE].
- [16] Yannick Ulrich, Djuna Croon, Jeremy Sakstein, and Samuel McDermott, “Multi-Generational Black Hole Population Analysis with an Astrophysically Informed Mass Function,” (2024), arXiv:2406.06109 [astro-ph.HE].
- [17] Mehdi El Bouhaddouti and Ilias Cholis, “On the mass distribution of the LIGO-Virgo-KAGRA events,” *Phys. Rev. D* **111**, 043020 (2025), arXiv:2409.00179 [astro-ph.CO].
- [18] Yin-Jie Li, Shao-Peng Tang, Yuan-Zhu Wang, and Yi-Zhong Fan, “Multispectral Sirens: Gravitational-wave Cosmology with (Multi-) Subpopulations of Binary Black Holes,” *Astrophys. J.* **976**, 153 (2024), arXiv:2406.11607 [astro-ph.CO].
- [19] Vasco Gennari, Simone Mastrogiovanni, Nicola Tamanini, Sylvain Marsat, and Grégoire Pierra, “Searching for additional structure and redshift evolution in the observed binary black hole population with a parametric time-dependent mass distribution,” *Phys. Rev. D* **111**, 123046 (2025), arXiv:2502.20445 [gr-qc].
- [20] A. G. Abac *et al.* (LIGO Scientific, VIRGO, KAGRA), “GWTC-4.0: Population Properties of Merging Compact Binaries,” (2025), arXiv:2508.18083 [astro-ph.HE].
- [21] Chris L. Fryer and Vassiliki Kalogera, “Theoretical black hole mass distributions,” *Astrophys. J.* **554**, 548–560 (2001), arXiv:astro-ph/9911312.
- [22] Krzysztof Belczynski, Michal Dominik, Tomasz Bulik, Richard O’Shaughnessy, Chris Fryer, and Daniel E. Holz, “The Effect of Metallicity on the Detection Prospects for Gravitational Waves,” *Astrophys. J. Lett.* **715**, L138–L141 (2010), arXiv:1004.0386 [astro-ph.HE].
- [23] Krzysztof Belczynski, Tomasz Bulik, Chris L. Fryer, Ashley Ruiter, Francesca Valsecchi, Jorick S. Vink, and Jarrod R. Hurley, “On the Maximum Mass of Stellar Black Holes,” *Astrophys. J.* **714**, 1217–1226 (2010), arXiv:0904.2784 [astro-ph.SR].
- [24] Chris L. Fryer, Krzysztof Belczynski, Grzegorz Wiktorowicz, Michal Dominik, Vicky Kalogera, and Daniel E. Holz,

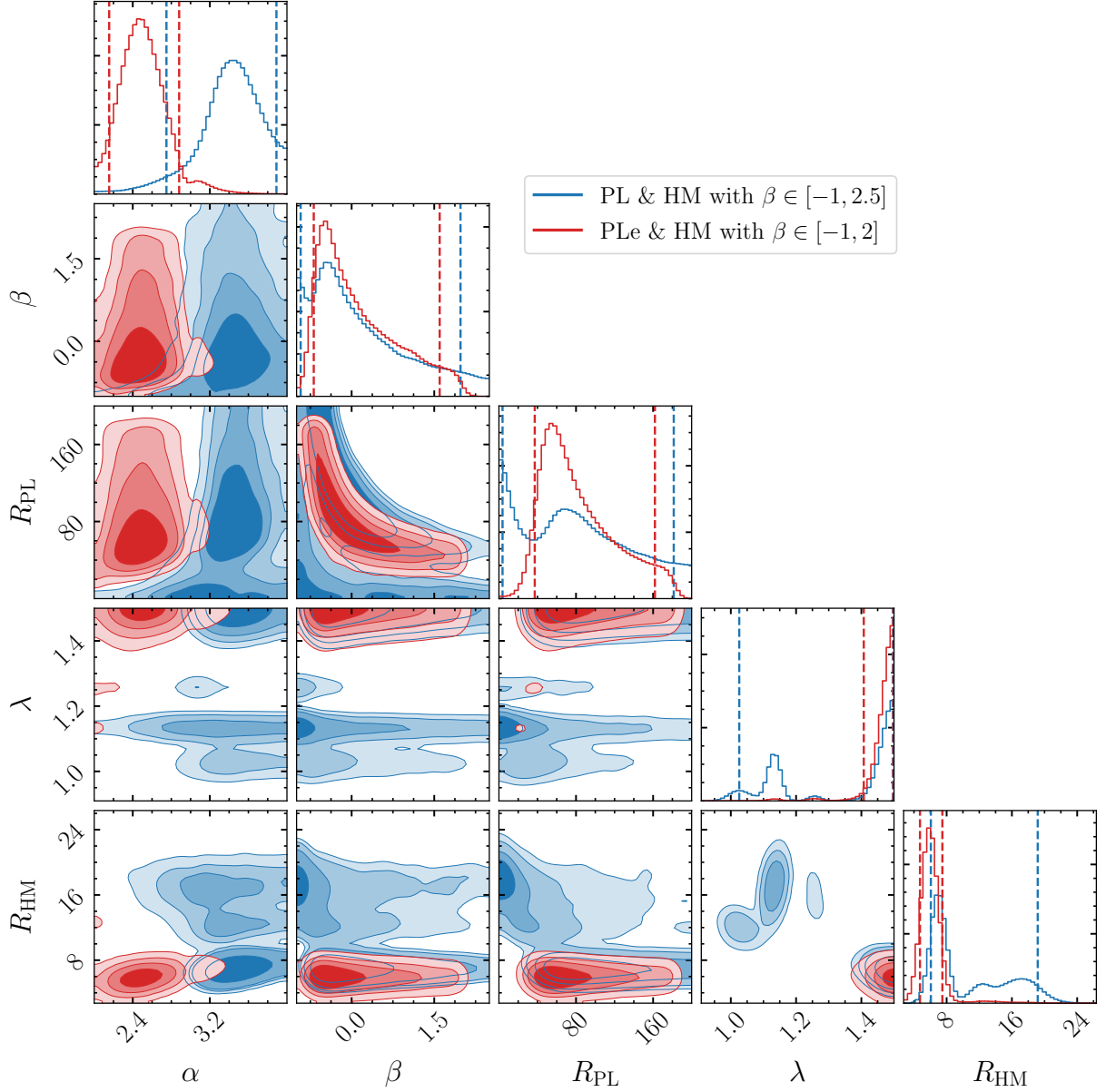


FIG. 13. Corner plot similar to that of Fig. 6, but with prior assumption on $-1 \leq \beta$.

- “Compact Remnant Mass Function: Dependence on the Explosion Mechanism and Metallicity,” *Astrophys. J.* **749**, 91 (2012), arXiv:1110.1726 [astro-ph.SR].
- [25] Carl L. Rodriguez, Sourav Chatterjee, and Frederic A. Rasio, “Binary Black Hole Mergers from Globular Clusters: Masses, Merger Rates, and the Impact of Stellar Evolution,” *Phys. Rev. D* **93**, 084029 (2016), arXiv:1602.02444 [astro-ph.HE].
- [26] Félix Mirabel, “The formation of stellar black holes,” *New Astronomy Reviews* **78**, 1–15 (2017).
- [27] Fabio Antonini and Frederic A. Rasio, “Merging black hole binaries in galactic nuclei: implications for advanced-LIGO detections,” *Astrophys. J.* **831**, 187 (2016), arXiv:1606.04889 [astro-ph.HE].
- [28] Maya Fishbach, Daniel E. Holz, and Ben Farr, “Are LIGO’s Black Holes Made From Smaller Black Holes?” *Astrophys. J. Lett.* **840**, L24 (2017), arXiv:1703.06869 [astro-ph.HE].
- [29] Davide Gerosa and Emanuele Berti, “Are merging black holes born from stellar collapse or previous mergers?” *Phys. Rev. D* **95**, 124046 (2017), arXiv:1703.06223 [gr-qc].
- [30] Ely D. Kovetz, Ilias Cholis, Marc Kamionkowski, and Joseph Silk, “Limits on Runaway Growth of Intermediate Mass Black Holes from Advanced LIGO,” *Phys. Rev. D* **97**, 123003 (2018), arXiv:1803.00568 [astro-ph.HE].
- [31] Fabio Antonini, Mark Gieles, and Alessia Gualandris, “Black hole growth through hierarchical black hole mergers in dense star clusters: implications for gravitational wave detections,” *Mon. Not. Roy. Astron. Soc.* **486**, 5008–5021 (2019), arXiv:1811.03640 [astro-ph.HE].
- [32] K. Kritos, V. De Luca, G. Franciolini, A. Keha-

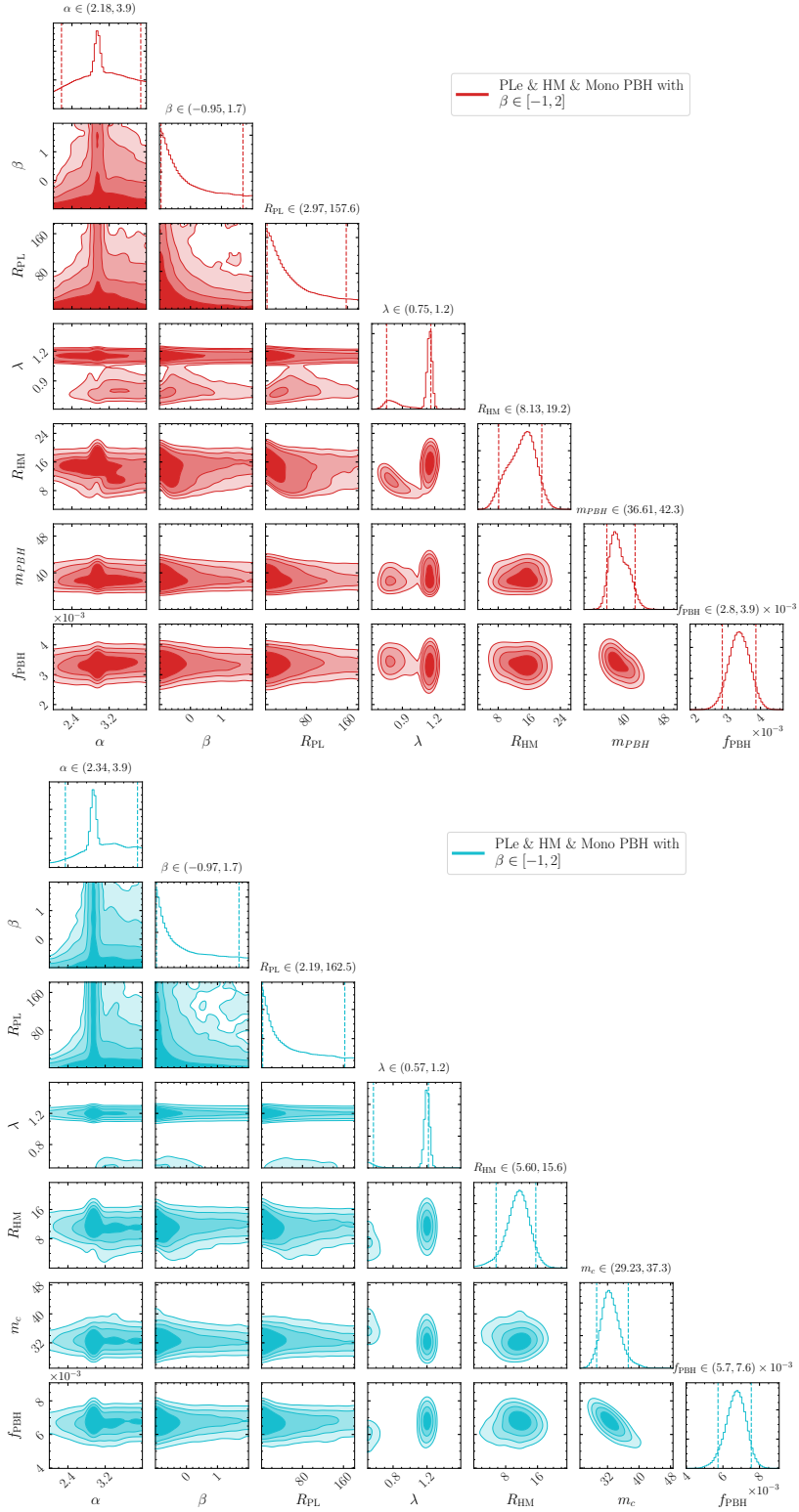


FIG. 14. Corner plot as in Fig. 8, (top panel) and Fig. 9, (bottom panel) representing the fit parameter values for PLe & HM & Mono PBH (top) and PLe & HM & Lognorm PBH (bottom) population synthesis models, for a prior on $-1 \leq \beta$.

- gias, and A. Riotto, “The Astro-Primordial Black Hole Merger Rates: a Reappraisal,” *JCAP* **05**, 039 (2021), [arXiv:2012.03585 \[gr-qc\]](#).
- [33] Rujuta A. Purohit, Giacomo Fragione, Frederic A. Rasio, Grayson C. Petter, and Ryan C. Hickox, “Binary Black Hole Mergers and Intermediate-mass Black Holes in Dense Star Clusters with Collisional Runaways,” *Astron. J.* **167**, 191 (2024), [arXiv:2401.06731 \[astro-ph.GA\]](#).
- [34] Giacomo Fragione and Frederic A. Rasio, “Demographics of Hierarchical Black Hole Mergers in Dense Star Clusters,” *Astrophys. J.* **951**, 129 (2023), [arXiv:2302.11613 \[astro-ph.GA\]](#).
- [35] Misao Sasaki, Teruaki Suyama, Takahiro Tanaka, and Shuichiro Yokoyama, “Primordial Black Hole Scenario for the Gravitational-Wave Event GW150914,” *Phys. Rev. Lett.* **117**, 061101 (2016), [Erratum: *Phys.Rev.Lett.* 121, 059901 (2018)], [arXiv:1603.08338 \[astro-ph.CO\]](#).
- [36] Simeon Bird, Ilias Cholis, Julian B. Muñoz, Yacine Ali-Haïmoud, Marc Kamionkowski, Ely D. Kovetz, Alvise Raccanelli, and Adam G. Riess, “Did LIGO detect dark matter?” *Phys. Rev. Lett.* **116**, 201301 (2016), [arXiv:1603.00464 \[astro-ph.CO\]](#).
- [37] Ely D. Kovetz, Ilias Cholis, Patrick C. Breysse, and Marc Kamionkowski, “Black hole mass function from gravitational wave measurements,” *Phys. Rev. D* **95**, 103010 (2017), [arXiv:1611.01157 \[astro-ph.CO\]](#).
- [38] Ely D. Kovetz, “Probing Primordial-Black-Hole Dark Matter with Gravitational Waves,” *Phys. Rev. Lett.* **119**, 131301 (2017), [arXiv:1705.09182 \[astro-ph.CO\]](#).
- [39] Bradley J. Kavanagh, Daniele Gaggero, and Gianfranco Bertone, “Merger rate of a subdominant population of primordial black holes,” *Phys. Rev. D* **98**, 023536 (2018), [arXiv:1805.09034 \[astro-ph.CO\]](#).
- [40] Sebastien Clesse and Juan Garcia-Bellido, “GW190425, GW190521 and GW190814: Three candidate mergers of primordial black holes from the QCD epoch,” *Phys. Dark Univ.* **38**, 101111 (2022), [arXiv:2007.06481 \[astro-ph.CO\]](#).
- [41] Gabriele Franciolini, Konstantinos Kritos, Emanuele Berti, and Joseph Silk, “Primordial black hole mergers from three-body interactions,” *Phys. Rev. D* **106**, 083529 (2022), [arXiv:2205.15340 \[astro-ph.CO\]](#).
- [42] Valerio De Luca, Gabriele Franciolini, and Antonio Riotto, “Heavy Primordial Black Holes from Strongly Clustered Light Black Holes,” *Phys. Rev. Lett.* **130**, 171401 (2023), [arXiv:2210.14171 \[astro-ph.CO\]](#).
- [43] Bernard Carr, Sebastien Clesse, Juan Garcia-Bellido, Michael Hawkins, and Florian Kuhnel, “Observational evidence for primordial black holes: A positivist perspective,” *Phys. Rept.* **1054**, 1–68 (2024), [arXiv:2306.03903 \[astro-ph.CO\]](#).
- [44] Martti Raidal, Ville Vaskonen, and Hardi Veermäe, “Formation of Primordial Black Hole Binaries and Their Merger Rates,” in *Primordial Black Holes*, edited by Christian Byrnes, Gabriele Franciolini, Tomohiro Harada, Paolo Pani, and Misao Sasaki (2025) [arXiv:2404.08416 \[astro-ph.CO\]](#).
- [45] Muhsin Aljaf and Ilias Cholis, “Simulating binary primordial black hole mergers in dark matter halos,” *Phys. Rev. D* **111**, 063020 (2025).
- [46] Bernard Carr and Florian Kuhnel, “Primordial Black Holes,” (2025), [arXiv:2502.15279 \[astro-ph.CO\]](#).
- [47] Ataru Tanikawa, “Contribution of population III stars to merging binary black holes,” *Rev. Mod. Plasma Phys.* **8**, 13 (2024), [arXiv:2403.04389 \[astro-ph.HE\]](#).
- [48] Grzegorz Wiktorowicz, Łukasz Wyrzykowski, Martyna Chruslinska, Jakub Klencki, Krzysztof A. Rybicki, and Krzysztof Belczynski, “Populations of stellar mass Black holes from binary systems,” (2019), [10.3847/1538-4357/ab45e6](#), [arXiv:1907.11431 \[astro-ph.HE\]](#).
- [49] M. Mapelli, L. Zampieri, E. Ripamonti, and A. Bressan, “Dynamics of stellar black holes in young star clusters with different metallicities - I. Implications for X-ray binaries,” *Mon. Not. Roy. Astron. Soc.* **429**, 2298 (2013), [arXiv:1211.6441 \[astro-ph.HE\]](#).
- [50] Meagan Morscher, Bharath Pattabiraman, Carl Rodriguez, Frederic A. Rasio, and Stefan Umbreit, “The Dynamical Evolution of Stellar Black Holes in Globular Clusters,” *Astrophys. J.* **800**, 9 (2015), [arXiv:1409.0866 \[astro-ph.GA\]](#).
- [51] Brunetto Marco Ziosi, Michela Mapelli, Marica Branchesi, and Giuseppe Tormen, “Dynamics of stellar black holes in young star clusters with different metallicities - II. Black hole-black hole binaries,” *Mon. Not. Roy. Astron. Soc.* **441**, 3703–3717 (2014), [arXiv:1404.7147 \[astro-ph.GA\]](#).
- [52] Thomas O. Kimpson, Mario Spera, Michela Mapelli, and Brunetto M. Ziosi, “Hierarchical black hole triples in young star clusters: impact of Kozai–Lidov resonance on mergers,” *Mon. Not. Roy. Astron. Soc.* **463**, 2443–2452 (2016), [arXiv:1608.05422 \[astro-ph.GA\]](#).
- [53] Pavel Kroupa, “On the variation of the initial mass function,” *Mon. Not. Roy. Astron. Soc.* **322**, 231 (2001), [arXiv:astro-ph/0009005](#).
- [54] S. E. Woosley and Alexander Heger, “The Pair-Instability Mass Gap for Black Holes,” *Astrophys. J. Lett.* **912**, L31 (2021), [arXiv:2103.07933 \[astro-ph.SR\]](#).
- [55] Guo-Peng Li and Xi-Long Fan, “The Origin Channels of Hierarchical Binary Black Hole Mergers in the LIGO–Virgo–KAGRA O1, O2, and O3 Runs,” *Astrophys. J.* **981**, 177 (2025), [arXiv:2411.09195 \[astro-ph.HE\]](#).
- [56] R. Abbott *et al.* (KAGRA, VIRGO, LIGO Scientific), “Population of Merging Compact Binaries Inferred Using Gravitational Waves through GWTC-3,” *Phys. Rev. X* **13**, 011048 (2023), [arXiv:2111.03634 \[astro-ph.HE\]](#).
- [57] Claire S. Ye, Maya Fishbach, Kyle Kremer, and Marta Reina-Campos, “Mass Distribution of Binary Black Hole Mergers from Young and Old Dense Star Clusters,” (2025), [arXiv:2507.07183 \[astro-ph.HE\]](#).
- [58] Stephen Hawking, “Gravitationally collapsed objects of very low mass,” *Mon. Not. Roy. Astron. Soc.* **152**, 75 (1971).
- [59] Ya. B. Zel’dovich and I. D. Novikov, “The Hypothesis of Cores Retarded during Expansion and the Hot Cosmological Model,” *Sov. Astron.* **10**, 602 (1967).
- [60] G. F. Chapline, “Cosmological effects of primordial black holes,” *Nature (London)* **253**, 251–252 (1975).
- [61] Bernard Carr, Florian Kuhnel, and Marit Sandstad, “Primordial Black Holes as Dark Matter,” *Phys. Rev. D* **94**, 083504 (2016), [arXiv:1607.06077 \[astro-ph.CO\]](#).
- [62] B. P. Abbott *et al.* (LIGO Scientific, Virgo), “Observation of Gravitational Waves from a Binary Black Hole Merger,” *Phys. Rev. Lett.* **116**, 061102 (2016), [arXiv:1602.03837 \[gr-qc\]](#).
- [63] Muhsin Aljaf and Ilias Cholis, “The Merger Rate of Primordial Black Holes,” (2025), [arXiv:2512.12227 \[astro-ph.HE\]](#).
- [64] The LIGO Scientific Collaboration *et al.*, “Advanced ligo,” *Classical and Quantum Gravity* **32**, 074001 (2015).
- [65] LIGO Scientific Collaboration, Virgo Collaboration, and

- KAGRA Collaboration, “Gwtc-3: Compact binary coalescences observed by ligo and virgo during the second part of the third observing run — parameter estimation data release,” (2023).
- [66] LIGO Scientific Collaboration, Virgo Collaboration, and KAGRA Collaboration, “Gwtc-4.0: Parameter estimation data release,” (2025).
- [67] Hasan Yüksel, Matthew D. Kistler, John F. Beacom, and Andrew M. Hopkins, “Revealing the high-redshift star formation rate with gamma-ray bursts,” *The Astrophysical Journal* **683**, L5–L8 (2008).
- [68] Piero Madau and Mark Dickinson, “Cosmic star-formation history,” *Annual Review of Astronomy and Astrophysics* **52**, 415–486 (2014).
- [69] Yacine Ali-Haïmoud, Ely D. Kovetz, and Marc Kamionkowski, “Merger rate of primordial black-hole binaries,” *Phys. Rev. D* **96**, 123523 (2017), arXiv:1709.06576 [astro-ph.CO].
- [70] Ilias Cholis, Ely D. Kovetz, Yacine Ali-Haïmoud, Simeon Bird, Marc Kamionkowski, Julian B. Muñoz, and Alvise Raccanelli, “Orbital eccentricities in primordial black hole binaries,” *Phys. Rev. D* **94**, 084013 (2016), arXiv:1606.07437 [astro-ph.HE].
- [71] P. C. Peters, “Gravitational Radiation and the Motion of Two Point Masses,” *Physical Review* **136**, 1224–1232 (1964).
- [72] Steven Murray, Chris Power, and A. S. G. Robotham, “HMFcalc: An online tool for calculating dark matter halo mass functions,” *Astron. Comput.* **3-4**, 23–34 (2013), arXiv:1306.6721 [astro-ph.CO].
- [73] D. C. Heggie, “Binary evolution in stellar dynamics,” *Mon. Not. Roy. Astron. Soc.* **173**, 729–787 (1975).
- [74] James Binney and Scott Tremaine, *Galactic dynamics* (1987).
- [75] Gerald D. Quinlan, “The dynamical evolution of massive black hole binaries - I. hardening in a fixed stellar background,” *New Astron.* **1**, 35–56 (1996), arXiv:astro-ph/9601092.
- [76] Alberto Sesana, Francesco Haardt, and Piero Madau, “Interaction of massive black hole binaries with their stellar environment. 1. Ejection of hypervelocity stars,” *Astrophys. J.* **651**, 392–400 (2006), arXiv:astro-ph/0604299.
- [77] Julio F. Navarro, Carlos S. Frenk, and Simon D. M. White, “The Structure of cold dark matter halos,” *Astrophys. J.* **462**, 563–575 (1996), arXiv:astro-ph/9508025.
- [78] Camila A. Correa, J. Stuart B. Wyithe, Joop Schaye, and Alan R. Duffy, “The accretion history of dark matter haloes – II. The connections with the mass power spectrum and the density profile,” *Mon. Not. Roy. Astron. Soc.* **450**, 1521–1537 (2015), arXiv:1501.04382 [astro-ph.CO].
- [79] Mehdi El Bouhaddouti, Muhsin Aljaf, and Ilias Cholis, “Conservative limits on primordial black holes from the LIGO-Virgo-KAGRA observations,” (2025), arXiv:2502.00144 [astro-ph.CO].
- [80] Éanna É. Flanagan and Scott A. Hughes, “Measuring gravitational waves from binary black hole coalescences. i. signal to noise for inspiral, merger, and ringdown,” *Physical Review D* **57**, 4535–4565 (1998).
- [81] Daniel Foreman-Mackey, David W. Hogg, Dustin Lang, and Jonathan Goodman, “emcee: The MCMC Hammer,” *Publications of the Astronomical Society of the Pacific* **125**, 306 (2013), arXiv:1202.3665 [astro-ph.IM].
- [82] Will Vausden, Will M. Farr, and Ilya Mandel, “ptemcee: A parallel-tempered version of emcee,” *Astrophysics Source Code Library*, record ascl:2101.006 (2021), ascl:2101.006.
- [83] Aidan Mai, Kyle Kremer, and Fulya Kiroglu, “Shadows of the Colossus: Hierarchical Black Hole Mergers in a 10-million-body Globular Cluster Simulation,” (2025), arXiv:2510.21916 [astro-ph.GA].
- [84] Amanda Newton, Sanaea C. Rose, Fulya Kiroğlu, Bao-Minh Hoang, and Frederic A. Rasio, “Intermediate-Mass Black Hole Formation from Hierarchical Mergers in Galactic Nuclei,” arXiv e-prints, arXiv:2602.04176 (2026), arXiv:2602.04176 [astro-ph.GA].
- [85] Miguel Zumalacárregui and Uroš Seljak, “Limits on stellar-mass compact objects as dark matter from gravitational lensing of type ia supernovae,” *Physical Review Letters* **121** (2018), 10.1103/physrevlett.121.141101.
- [86] Timothy D. Brandt, “Constraints on macho dark matter from compact stellar systems in ultra-faint dwarf galaxies,” *The Astrophysical Journal Letters* **824**, L31 (2016).
- [87] Miguel A. Monroy-Rodríguez and Christine Allen, “The end of the macho era, revisited: New limits on macho masses from halo wide binaries,” *The Astrophysical Journal* **790**, 159 (2014).
- [88] Przemek Mróz, Andrzej Udalski, Michał K. Szymański, Mateusz Kapusta, Igor Soszyński, Łukasz Wyrzykowski, Paweł Pietrukowicz, Szymon Kozłowski, Radosław Poleski, Jan Skowron, Dorota Skowron, Krzysztof Ulaczyk, Mariusz Gromadzki, Krzysztof Rybicki, Patryk Iwanek, Marcin Wrona, and Milena Ratajczak, “Microlensing optical depth and event rate toward the large magellanic cloud based on 20 yr of ogle observations,” *The Astrophysical Journal Supplement Series* **273**, 4 (2024).
- [89] Przemek Mróz, Andrzej Udalski, Michał K. Szymański, Igor Soszyński, Łukasz Wyrzykowski, Paweł Pietrukowicz, Szymon Kozłowski, Radosław Poleski, Jan Skowron, Dorota Skowron, Krzysztof Ulaczyk, Mariusz Gromadzki, Krzysztof Rybicki, Patryk Iwanek, Marcin Wrona, and Milena Ratajczak, “No massive black holes in the milky way halo,” *Nature* **632**, 749–751 (2024).
- [90] Pasquale D. Serpico, Vivian Poulin, Derek Inman, and Kazunori Kohri, “Cosmic microwave background bounds on primordial black holes including dark matter halo accretion,” *Physical Review Research* **2** (2020), 10.1103/physrevresearch.2.023204.
- [91] P. Tisserand, L. Le Guillou, C. Afonso, J. N. Albert, J. Andersen, R. Ansari, É. Aubourg, P. Bareyre, J. P. Beaulieu, X. Charlot, C. Coutures, R. Ferlet, P. Fouqué, J. F. Gliesenstein, B. Goldman, A. Gould, D. Graff, M. Gros, J. Haissinski, C. Hamadache, J. de Kat, T. Lasserre, É. Lesquoy, C. Loup, C. Magneville, J. B. Marquette, É. Maurice, A. Maury, A. Milsztajn, M. Moniez, N. Palanque-Delabrouille, O. Perdureau, Y. R. Rahal, J. Rich, M. Spiro, A. Vidal-Madjar, and L. Vigroux, “Limits on the macho content of the galactic halo from the eros-2 survey of the magellanic clouds,” *Astronomy and Astrophysics* **469**, 387–404 (2007).
- [92] A. Alcock, R. A. Allsman, D. R. Alves, T. S. Axelrod, A. C. Becker, D. P. Bennett, K. H. Cook, N. Dalal, A. J. Drake, K. C. Freeman, M. Geha, K. Griest, M. J. Lehner, S. L. Marshall, D. Minniti, C. A. Nelson, B. A. Peterson, P. Popowski, M. R. Pratt, P. J. Quinn, C. W. Stubbs, W. Sutherland, A. B. Tomaney, T. Vandehei, D. L. Welch, and (The MACHO Collaboration), “Macho project limits

- on black hole dark matter in the 1-30 solar mass range,” *The Astrophysical Journal* **550**, L169 (2001).
- [93] Bernard Carr, Kazunori Kohri, Yuuiti Sendouda, and Jun’ichi Yokoyama, “Constraints on primordial black holes,” *Reports on Progress in Physics* **84**, 116902 (2021).
- [94] Anne M. Green and Bradley J. Kavanagh, “Primordial Black Holes as a dark matter candidate,” *J. Phys. G* **48**, 043001 (2021), [arXiv:2007.10722 \[astro-ph.CO\]](#).
- [95] Bradley J. Kavanagh, “bradkav/pbhbounds: Release version,” (2019).
- [96] Anne M. Green, “Primordial black hole stellar microlensing constraints: understanding their dependence on the density and velocity distributions,” *JCAP* **04**, 023 (2025), [arXiv:2501.02610 \[astro-ph.GA\]](#).
- [97] Emanuele Berti, Francesco Crescimbeni, Gabriele Franciolini, Simone Mastrogiovanni, Paolo Pani, and Grégoire Pierra, “Inferring black hole formation channels in GWTC-4.0 via parametric mass-spin correlations derived from first principles,” (2025), [arXiv:2512.03152 \[gr-qc\]](#).